12 Cosmic Microwave Background Anisotropy

The cosmic microwave background (CMB) is isotropic to a high degree. This tells us that the early universe was rather homogeneous at the time ($t = t_{\mathrm{dec}}$) the CMB was formed. However, with precise measurements we can detect a low-level anisotropy in the CMB which reflects the small perturbations in the early universe.

This anisotropy was first detected by the American COBE satellite in 1992, which mapped the whole sky in three microwave frequencies. The angular resolution of COBE was rather poor, 7°, meaning that only features larger than this were detected. Measurements with better resolution, but covering only small parts of the sky were then performed using instruments carried by balloons to the upper atmosphere, and ground-based detectors located at high altitudes.

The best CMB anisotropy data to date, covering the whole sky, has been provided by the WMAP satellite, in orbit around the L2 point of the Sun-Earth system, 1.5 million kilometers from the Earth in the anti-Sun direction. The satellite was launched by NASA in June, 2001, and in February 2003 the WMAP team published their results from the first year of measurements (WMAP1 [1]).

It takes WMAP 6 months to observe the entire sky. The satellite repeats these observations year after year, and the results become gradually more accurate, since the effects of instrument noise average out better when there are more observations.

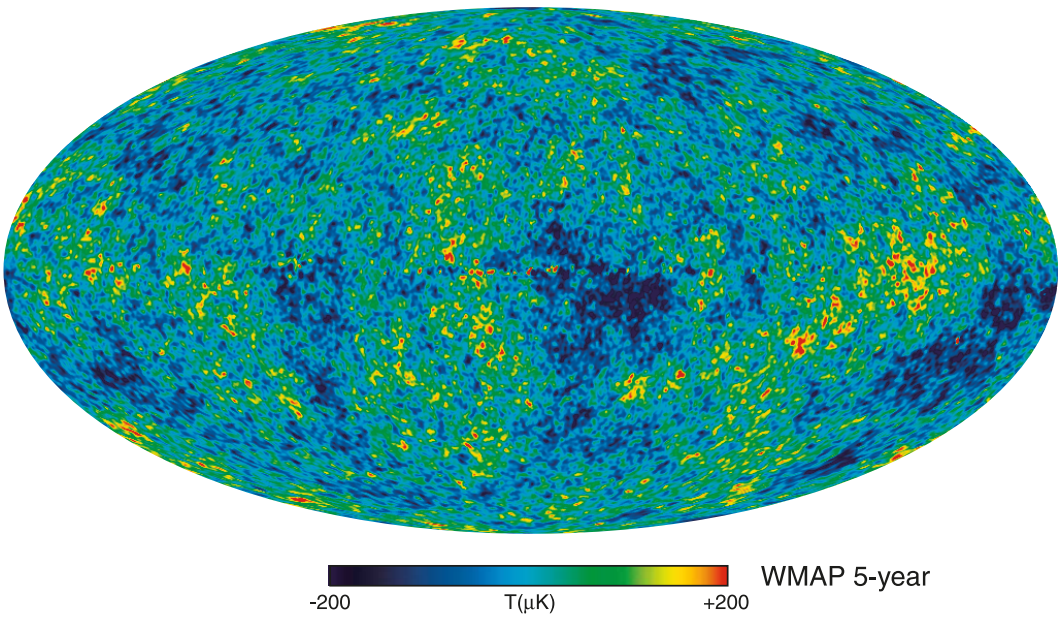

Figure 1: Cosmic microwave background according to WMAP 5-year results (NASA/WMAP Science Team).

Figure 1 shows the observed variation $\left(\frac{\delta T}{T}\right)_{\mathrm{obs}}$ in the temperature of the CMB on the sky (yellow and red mean hotter than average, blue means colder than average).

The photons we see as the CMB have traveled to us from where our past light cone intersects the hypersurface corresponding to the time $t = t_{\mathrm{dec}}$ of photon decoupling. This intersection forms a sphere which we shall call the *last scattering*

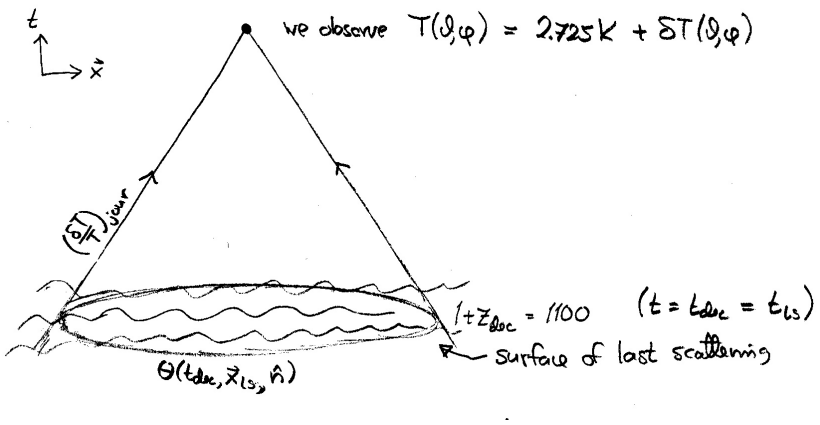

Figure 2: The observed CMB temperature anisotropy gets a contribution from the last scattering surface, $(\delta T/T)_{\rm intr} = \Theta(t_{\rm dec}, \boldsymbol{x}_{\rm ls}, \hat{\boldsymbol{n}})$ and from along the photon's journey to us, $(\delta T/T)_{\rm jour}$.

surface.[1] We are at the center of this sphere, except that timewise the sphere is located in the past.

The observed temperature anisotropy is due to two contributions, an *intrinsic* temperature variation at the surface of last scattering and a variation in the redshift the photons have suffered during their "journey" to us,

$$\left(\frac{\delta T}{T}\right)_{\rm obs} = \left(\frac{\delta T}{T}\right)_{\rm intr} + \left(\frac{\delta T}{T}\right)_{\rm jour} . \tag{1}$$

See Fig. 2.

The first term, $\left(\frac{\delta T}{T}\right)_{\rm intr}$ represents the temperature variation of the photon gas at $t = t_{\rm dec}$. (We also include in it the Doppler effect from the motion of this photon gas.) At that time the larger scales we see in the CMB sky were still outside the horizon, so we have to pay attention to the gauge choice. In fact, the separation of $\delta T/T$ into two components in Eq. (1) is gauge-dependent. If the time slice $t = t_{\rm dec}$ dips further into the past in some location, it finds a higher temperature, but the photons from there also have then a longer way to go and suffer a larger redshift, so that the two effects balance each other. We can calculate in any gauge we want, getting different results for $(\delta T/T)_{\rm intr}$ and $(\delta T/T)_{\rm jour}$ depending on the gauge, but their sum $(\delta T/T)_{\rm obs}$ is gauge-independent. (It has to be, being an observed quantity).

One might think that $(\delta T/T)_{\rm intr}$ should be equal to zero, since in our earlier discussion of recombination and decoupling we identified decoupling with a particular temperature $T_{\rm dec} \sim 3000$ K. This kind of thinking corresponds to a particular gauge choice where the $t = t_{\rm dec}$ time slice coincides with the $T = T_{\rm dec}$ hypersurface. In this gauge $(\delta T/T)_{\rm intr} = 0$, except for the Doppler effect (we are not going to use this gauge). Anyway, it is not true that all photons have their last scattering exactly when $T = T_{\rm dec}$. Rather they occur during a rather large temperature interval and time period. The zeroth-order (background) time evolution of the temperature of the photon distribution is the same before and after last scattering, $T \propto a^{-1}$, so it

[1] Or the *last scattering sphere*. "Last scattering surface" often refers to the entire $t = t_{\rm dec}$ time slice.

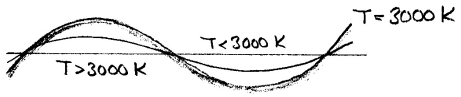

Figure 3: Depending on the gauge, the $T_{\rm dec}$ = const. surface may, or (usually) may not coincide with the $t = t_{\rm dec}$ time slice.

does not matter how we draw the artificial separation line, the time slice $t = t_{\rm dec}$ separating the fluid and free particle treatments of the photons. See Fig. 3.

12.1 Multipole Analysis

The CMB temperature anisotropy is a function over a sphere. In analogy to the Fourier expansion of 3-dim space, we separate out the contributions of different angular scales by doing a multipole expansion,

$$\frac{\delta T}{T_0}(\theta,\phi) = \sum a_{\ell m} Y_{\ell m}(\theta,\phi) \tag{2}$$

where the sum runs over $l = 1, 2, \ldots \infty$ and $m = -l, \ldots, l$, giving $2\ell + 1$ values of m for each ℓ. The functions $Y_{\ell m}(\theta,\phi)$ are the *spherical harmonics* (see Fig. 4), which form an orthonormal set of functions over the sphere, so that we can calculate the multipole coefficients $a_{\ell m}$ from

$$a_{\ell m} = \int Y^*_{\ell m}(\theta,\phi)\frac{\delta T}{T_0}(\theta,\phi)d\Omega\,. \tag{3}$$

Definition (2) gives dimensionless $a_{\ell m}$. Often they are defined without the $T_0 = 2.725$ K in Eq. (2), and then they have the dimension of temperature and are usually given in units of μK.

The sum begins at $\ell = 1$, since Y_{00} = const. and therefore we must have $a_{00} = 0$ for a quantity which represents a deviation from average. The dipole part, $\ell = 1$, is dominated by the Doppler effect due to the motion of the solar system with respect to the last scattering surface, and we cannot separate out from it the *cosmological dipole* caused by large scale perturbations. Therefore we are here interested only in the $\ell \geq 2$ part of the expansion.

Another notation for $Y_{\ell m}(\theta,\phi)$ is $Y_{\ell m}(\hat{\boldsymbol{n}})$, where $\hat{\boldsymbol{n}}$ is a unit vector whose direction is specified by the angles θ and ϕ.

12.1.1 Spherical Harmonics

We list here some useful properties of the spherical harmonics.

They are orthonormal functions on the sphere, so that

$$\int d\Omega\; Y_{\ell m}(\theta,\phi)Y^*_{\ell' m'}(\theta,\phi) = \delta_{\ell\ell'}\delta_{mm'}\,. \tag{4}$$

Summing over the m corresponding to the same multipole number ℓ we have the *closure relation*

$$\sum_m |Y_{\ell m}(\theta,\phi)|^2 = \frac{2\ell+1}{4\pi}\,. \tag{5}$$

We shall also need the expansion of a plane wave in terms of spherical harmonics,

$$e^{i\boldsymbol{k}\cdot\boldsymbol{x}} = 4\pi \sum_{\ell m} i^\ell j_\ell(kx) Y_{\ell m}(\hat{\boldsymbol{x}}) Y^*_{\ell m}(\hat{\boldsymbol{k}})\,. \tag{6}$$

Here $\hat{\boldsymbol{x}}$ and $\hat{\boldsymbol{k}}$ are the unit vectors in the directions of $\boldsymbol{x}$ and $\boldsymbol{k}$, and j_ℓ is the spherical Bessel function.

12.1.2 Theoretical angular power spectrum

The CMB anisotropy is due to the primordial perturbations, and therefore it reflects their Gaussian nature. Because one gets the values of the $a_{\ell m}$ from the other perturbation quantities through linear equations (in first-order perturbation theory), the $a_{\ell m}$ are also (complex) Gaussian random variables. Since they represent a deviation from the average temperature, their expectation value is zero,

$$\langle a_{\ell m}\rangle = 0\,, \tag{7}$$

and the quantity we want to calculate from theory is the variance $\langle |a_{\ell m}|^2\rangle$ to get a prediction for the typical size of the $a_{\ell m}$. The isotropic nature of the random process shows up in the $a_{\ell m}$ so that these expectation values depend only on ℓ not m. (The ℓ are related to the angular size of the anisotropy pattern, whereas the m are related to "orientation" or "pattern".) Since $\langle |a_{\ell m}|^2\rangle$ is independent of m, we can define

$$C_\ell \equiv \langle |a_{\ell m}|^2\rangle = \frac{1}{2\ell+1}\sum_m \langle |a_{\ell m}|^2\rangle\,. \tag{8}$$

The different $a_{\ell m}$ are independent random variables, so that

$$\langle a_{\ell m} a^*_{\ell' m'}\rangle = \delta_{\ell\ell'}\delta_{mm'} C_\ell\,. \tag{9}$$

This function C_ℓ (of integers $l \geq 1$) is called the (theoretical) *angular power spectrum*. It is analogous to the power spectrum $\mathcal{P}(k)$ of density perturbations. For Gaussian perturbations, the C_ℓ contains all the statistical information about the CMB temperature anisotropy. And this is all we can predict from theory. Thus the analysis of the CMB anisotropy consists of calculating the angular power spectrum from the observed CMB (a map like Figure 1) and comparing it to the C_ℓ predicted by theory.[2]

Just like the 3-dim density power spectrum $\mathcal{P}(k)$ gives the contribution of scale k to the density variance $\langle \delta(\boldsymbol{x})^2\rangle$, the angular power spectrum C_ℓ is related to the contribution of multipole ℓ to the temperature variance,

$$\begin{aligned}
\left\langle \left(\frac{\delta T(\theta,\phi)}{T}\right)^2 \right\rangle &= \left\langle \sum_{\ell m} a_{\ell m} Y_{\ell m}(\theta,\phi) \sum_{\ell' m'} a^*_{\ell' m'} Y^*_{\ell' m'}(\theta,\phi) \right\rangle \\
&= \sum_{\ell\ell'}\sum_{mm'} Y_{\ell m}(\theta,\phi) Y^*_{\ell' m'}(\theta,\phi) \langle a_{\ell m} a^*_{\ell' m'}\rangle \\
&= \sum_\ell C_\ell \sum_m |Y_{\ell m}(\theta,\phi)|^2 = \sum_\ell \frac{2\ell+1}{4\pi} C_\ell\,,
\end{aligned} \tag{10}$$

[2] In addition to the temperature anisotropy, the CMB also has another property, its polarization. There are two additional power spectra related to the polarization, C_ℓ^E and C_ℓ^B, and one related to the correlation between temperature and polarization, C_ℓ^{TE}.

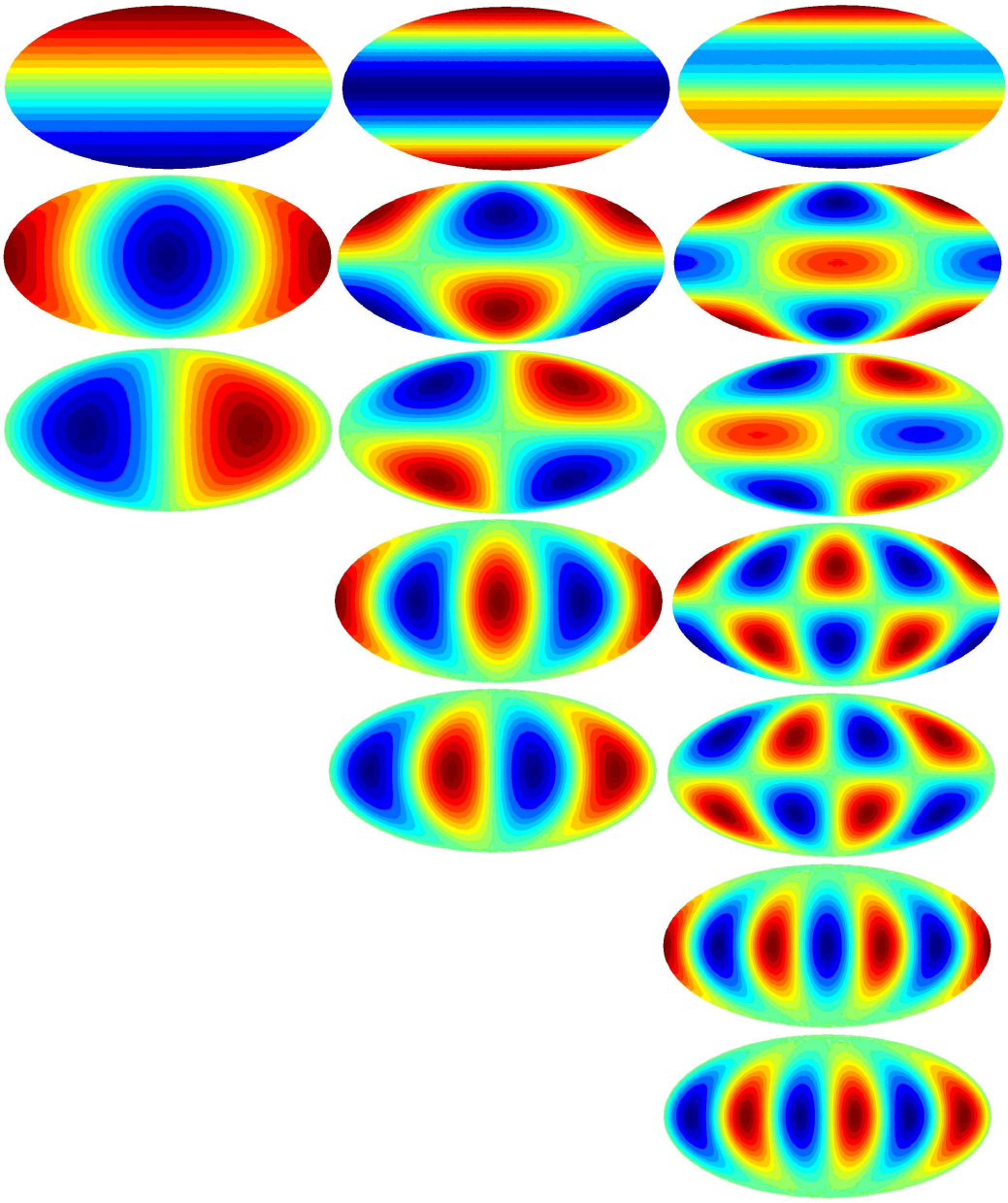

Figure 4: The three lowest multipoles $\ell = 1, 2, 3$ of spherical harmonics. Left column: Y_{10}, $\mathrm{Re}\, Y_{11}$, $\mathrm{Im}\, Y_{11}$. Middle column: Y_{20}, $\mathrm{Re}\, Y_{21}$, $\mathrm{Im}\, Y_{21}$, $\mathrm{Re}\, Y_{22}$, $\mathrm{Im}\, Y_{22}$. Right column: Y_{30}, $\mathrm{Re}\, Y_{31}$, $\mathrm{Im}\, Y_{31}$, $\mathrm{Re}\, Y_{32}$, $\mathrm{Im}\, Y_{32}$, $\mathrm{Re}\, Y_{33}$, $\mathrm{Im}\, Y_{33}$. Figure by Ville Heikkilä.

where we used Eq. (9) and the *closure relation*, Eq. (5)

Thus, if we plot $(2\ell+1)C_\ell/4\pi$ on a linear ℓ scale, or $\ell(2\ell+1)C_\ell/4\pi$ on a logarithmic ℓ scale, the area under the curve gives the temperature variance, i.e., the expectation value for the squared deviation from the average temperature. It has become customary to plot the angular power spectrum as $\ell(\ell+1)C_\ell/2\pi$, which is neither of these, but for large ℓ approximates the second case. The reason for this custom is explained later.

Eq. (10) represents the expectation value from theory and thus it is the same for all directions θ,ϕ. The actual, "realized", value of course varies from one direction θ,ϕ to another. We can imagine an ensemble of universes, otherwise like our own, but representing a different realization of the same random process of producing the primordial perturbations. Then $\langle\ \rangle$ represents the average over such an ensemble.

12.1.3 Observed angular power spectrum

Theory predicts expectation values $\langle|a_{\ell m}|^2\rangle$ from the random process responsible for the CMB anisotropy, but we can observe only one realization of this random process, the set $\{a_{\ell m}\}$ of our CMB sky. We define the *observed* angular power spectrum as the average

$$\widehat{C}_\ell = \frac{1}{2\ell+1}\sum_m |a_{\ell m}|^2 \tag{11}$$

of these observed values.

The variance of the observed temperature anisotropy is the average of $\left(\frac{\delta T(\theta,\phi)}{T}\right)^2$ over the celestial sphere,

$$\begin{aligned}\frac{1}{4\pi}\int\left[\frac{\delta T(\theta,\phi)}{T}\right]^2 d\Omega &= \frac{1}{4\pi}\int d\Omega \sum_{\ell m} a_{\ell m}Y_{\ell m}(\theta,\phi)\sum_{\ell' m'} a^*_{\ell' m'}Y^*_{\ell' m'}(\theta,\phi)\\ &= \frac{1}{4\pi}\sum_{\ell m}\sum_{\ell' m'} a_{\ell m}a^*_{\ell' m'}\underbrace{\int Y_{\ell m}(\theta,\phi)Y^*_{\ell' m'}(\theta,\phi)d\Omega}_{\delta_{\ell\ell'}\delta_{mm'}}\\ &= \frac{1}{4\pi}\sum_\ell \underbrace{\sum_m |a_{\ell m}|^2}_{(2\ell+1)\widehat{C}_\ell} = \sum_\ell \frac{2\ell+1}{4\pi}\widehat{C}_\ell\ .\end{aligned} \tag{12}$$

Contrast this with Eq. (10), which gives the variance of $\delta T/T$ at an arbitrary location on the sky over different realizations of the random process which produced the primordial perturbations; whereas Eq. (12) gives the variance of $\delta T/T$ of our given sky over the celestial sphere.

12.1.4 Cosmic Variance

The expectation value of the observed spectrum $\widehat{C}_\ell$ is equal to C_ℓ, the *theoretical* spectrum of Eq. (8), i.e.,

$$\langle\widehat{C}_\ell\rangle = C_\ell \quad\Rightarrow\quad \langle\widehat{C}_\ell - C_\ell\rangle = 0\,, \tag{13}$$

but its actual, realized, value is not, although we expect it to be close. The expected squared difference between $\widehat{C}_\ell$ and C_ℓ is called the *cosmic variance*. We can calculate

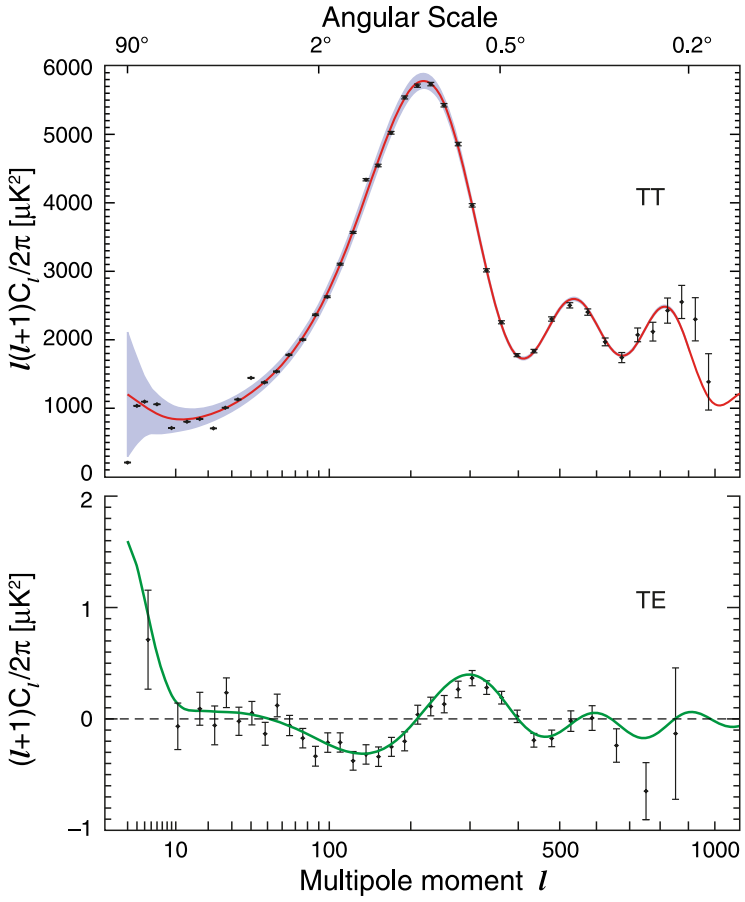

Figure 5: The observed angular power spectrum $\widehat{C}_\ell$ according to WMAP 5-year measurements (WMAP5 [3]). The observational results are the data points with error bars. The red curve is the theoretical C_ℓ from a best-fit model, and the blue band around it represents the cosmic variance corresponding to this C_ℓ. The bottom panel shows the observed temperature-polarization correlation spectrum $\widehat{C}_\ell^{TE}$. (NASA/WMAP Science Team).

it using the properties of (complex) Gaussian random variables (**exercise**). The answer is

$$\langle(\widehat{C}_\ell - C_\ell)^2\rangle = \frac{2}{2\ell+1}C_\ell^2\,. \tag{14}$$

We see that the expected relative difference between $\widehat{C}_\ell$ and C_ℓ is smaller for higher ℓ. This is because we have a larger (size $2\ell+1$) statistical sample of $a_{\ell m}$ available for calculating the $\widehat{C}_\ell$.

The cosmic variance limits the accuracy of comparison of CMB observations with theory, especially for large scales (low ℓ).

12.2 Multipoles and Scales

12.2.1 Rough Correspondence

The different multipole numbers ℓ correspond to different angular scales, low ℓ to large scales and high ℓ to small scales. Examination of the functions $Y_{\ell m}(\theta,\phi)$ reveals

that they have an oscillatory pattern on the sphere, so that there are typically ℓ "wavelengths" of oscillation around a full great circle of the sphere. See Fig. 6.

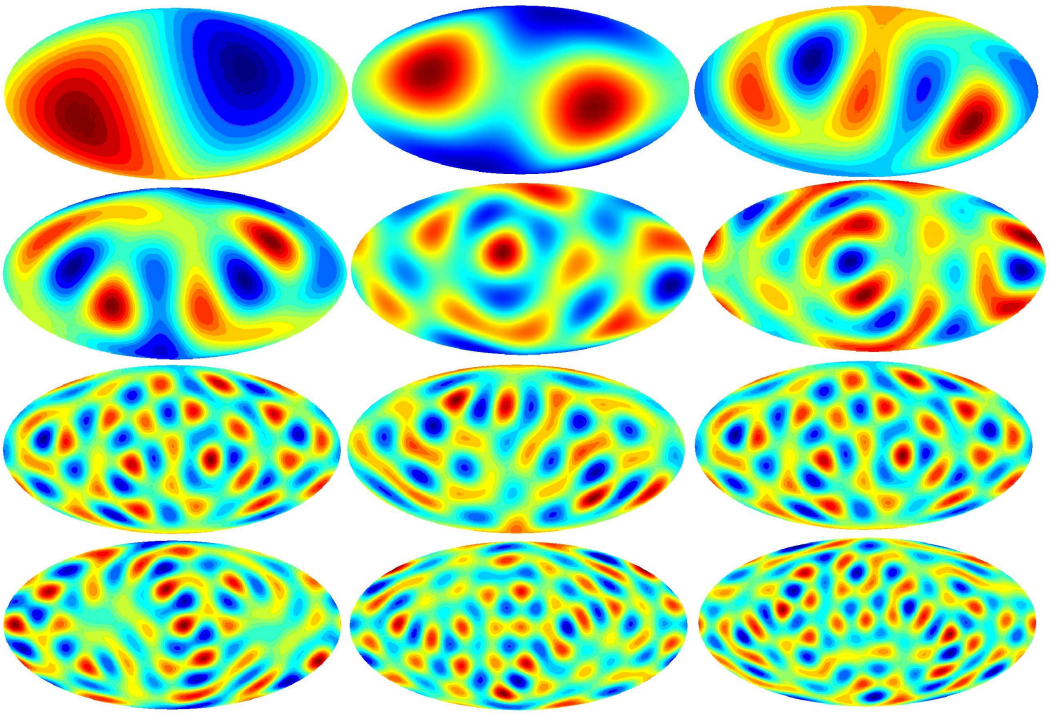

Figure 6: Randomly generated skies containing only a single multipole ℓ. Staring from top left: $\ell = 1$ (dipole only), 2 (quadrupole only), 3 (octupole only), 4, 5, 6, 7, 8, 9, 10, 11, 12. Figure by Ville Heikkilä.

Thus the angle corresponding to this wavelength is

$$\vartheta_\lambda = \frac{2\pi}{\ell} = \frac{360^\circ}{\ell}\,. \tag{15}$$

See Fig. 7. The angle corresponding to a "half-wavelength", i.e., the separation between a neighboring minimum and maximum is then

$$\vartheta_{\rm res} = \frac{\pi}{\ell} = \frac{180^\circ}{\ell}\,. \tag{16}$$

This is the angular resolution required of the microwave detector for it to be able to resolve the angular power spectrum up to this ℓ.

For example, COBE had an angular resolution of 7° allowing a measurement up to $\ell = 180/7 = 26$, WMAP had resolution 0.23° reaching to $\ell = 180/0.23 = 783$, and the European Planck satellite (launch in 2009) will have resolution $5'$, which will allow us to measure C_ℓ up to $\ell = 2160$.[3]

The angles on the sky are related to actual physical or comoving distances via the *angular diameter distance* d_A, defined as the ratio of the physical length (transverse to the line of sight) and the angle it covers (see Chapter 4),

$$d_A \equiv \frac{\lambda_{\rm phys}}{\vartheta}\,. \tag{17}$$

[3]In reality, there is no sharp cut-off at a particular ℓ, the observational error bars just blow up rapidly around this value of ℓ.

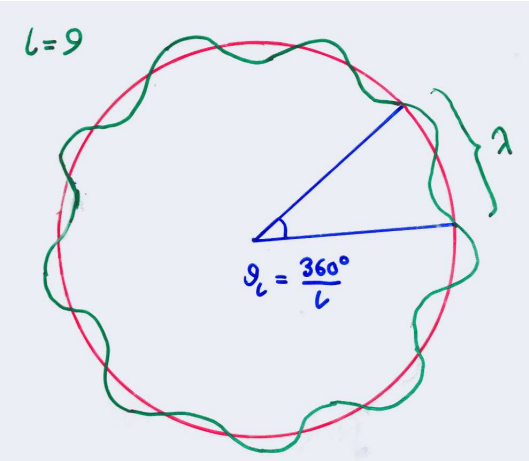

Figure 7: The rough correspondence between multipoles ℓ and angles.

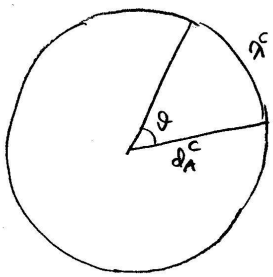

Figure 8: The comoving angular diameter distance relates the comoving size of an object and the angle in which we see it.

Likewise, we defined the *comoving angular diameter distance* d_A^c by

$$d_A^c \equiv \frac{\lambda^c}{\vartheta} \tag{18}$$

where $\lambda^c = (a_0/a)\lambda_{\rm phys} = (1+z)\lambda_{\rm phys}$ is the corresponding comoving length. Thus $d_A^c = (a_0/a)d_A = (1+z)d_A$. See Fig. 8

Consider now the Fourier modes of our earlier perturbation theory discussion. A mode with comoving wavenumber k has comoving wavelength $\lambda^c = 2\pi/k$. Thus this mode should show up as a pattern on the CMB sky with angular size

$$\vartheta_\lambda = \frac{\lambda^c}{d_A^c} = \frac{2\pi}{k d_A^c} = \frac{2\pi}{\ell}\,. \tag{19}$$

For the last equality we used the relation (15). From it we get that the modes with wavenumber k contribute mostly to multipoles around

$$\ell = k d_A^c\,. \tag{20}$$

12.2.2 Exact Treatment

The above matching of wavenumbers with multipoles was of course rather naive, for two reasons:

1. The description of a spherical harmonic $Y_{\ell m}$ having an "angular wavelength" of $2\pi/\ell$ is just a crude characterization. See Fig. 6.

2. The modes $\boldsymbol{k}$ are not wrapped around the sphere of last scattering, but the wave vector forms a different angle with the sphere at different places.

The following precise discussion applies only for the case of a flat universe ($K = 0$ Friedmann model as the background), where one can Fourier expand functions on a time slice. We start from the expansion of the plane wave in terms of spherical harmonics, for which we have the result, Eq. (6),

$$e^{i\boldsymbol{k}\cdot\boldsymbol{x}} = 4\pi \sum_{\ell m} i^\ell j_\ell(kx) Y_{\ell m}(\hat{\boldsymbol{x}}) Y^*_{\ell m}(\hat{\boldsymbol{k}})\,, \tag{21}$$

where j_ℓ is the spherical Bessel function.

Consider now some function

$$f(\boldsymbol{x}) = \sum_{\boldsymbol{k}} f_{\boldsymbol{k}} e^{i\boldsymbol{k}\cdot\boldsymbol{x}} \tag{22}$$

on the $t = t_{\rm dec}$ time slice. We want the multipole expansion of the values of this function on the last scattering sphere. See Fig. 9. These are the values $f(x\hat{\boldsymbol{x}})$, where $x \equiv |\boldsymbol{x}|$ has a constant value, the (comoving) radius of this sphere. Thus

$$\begin{aligned} a_{\ell m} &= \int d\Omega_x Y^*_{\ell m}(\hat{\boldsymbol{x}}) f(x\hat{\boldsymbol{x}}) \\ &= \sum_{\boldsymbol{k}} \int d\Omega_x Y^*_{\ell m}(\hat{\boldsymbol{x}}) f_{\boldsymbol{k}} e^{i\boldsymbol{k}\cdot\boldsymbol{x}} \\ &= 4\pi \sum_{\boldsymbol{k}} \sum_{\ell' m'} \int d\Omega_x f_{\boldsymbol{k}} Y^*_{\ell m}(\hat{\boldsymbol{x}}) i^{\ell'} j_{\ell'}(kx) Y_{\ell' m'}(\hat{\boldsymbol{x}}) Y^*_{\ell' m'}(\hat{\boldsymbol{k}}) \\ &= 4\pi i^\ell \sum_{\boldsymbol{k}} f_{\boldsymbol{k}} j_\ell(kx) Y^*_{\ell m}(\hat{\boldsymbol{k}})\,, \end{aligned} \tag{23}$$

where we used the orthonormality of the spherical harmonics. The corresponding result for a Fourier transform $f(\boldsymbol{k})$ is

$$a_{\ell m} = \frac{4\pi i^\ell}{(2\pi)^{3/2}} \int d^3k f(\boldsymbol{k}) j_\ell(kx) Y^*_{\ell m}(\hat{\boldsymbol{k}})\,. \tag{24}$$

The j_ℓ are oscillating functions with decreasing amplitude. For large values of ℓ the position of the first (and largest) maximum is near $kx = \ell$ (see Fig. 10).

Thus the $a_{\ell m}$ pick a large contribution from those Fourier modes $\boldsymbol{k}$ where

$$kx \sim \ell\,. \tag{25}$$

In a flat universe the comoving distance x (from our location to the sphere of last scattering) and the comoving angular diameter distance d_A^c are equal, so we can write this result as

$$kd_A^c \sim \ell\,. \tag{26}$$

The conclusion is that a given multipole ℓ acquires a contribution from modes with a range of wavenumbers, but most of the contribution comes from near the value given by Eq. (20). This concentration is tighter for larger ℓ.

We shall use Eq. (20) for qualitative purposes in the following discussion.

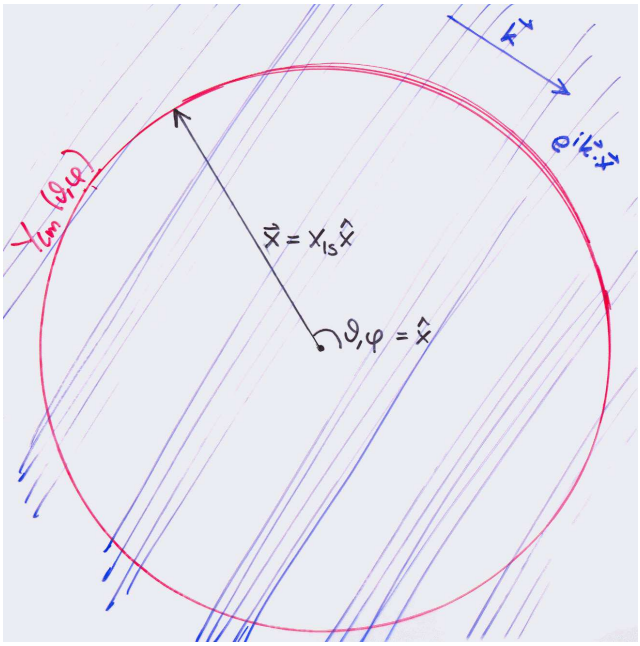

Figure 9: A plane wave intersecting the last scattering sphere.

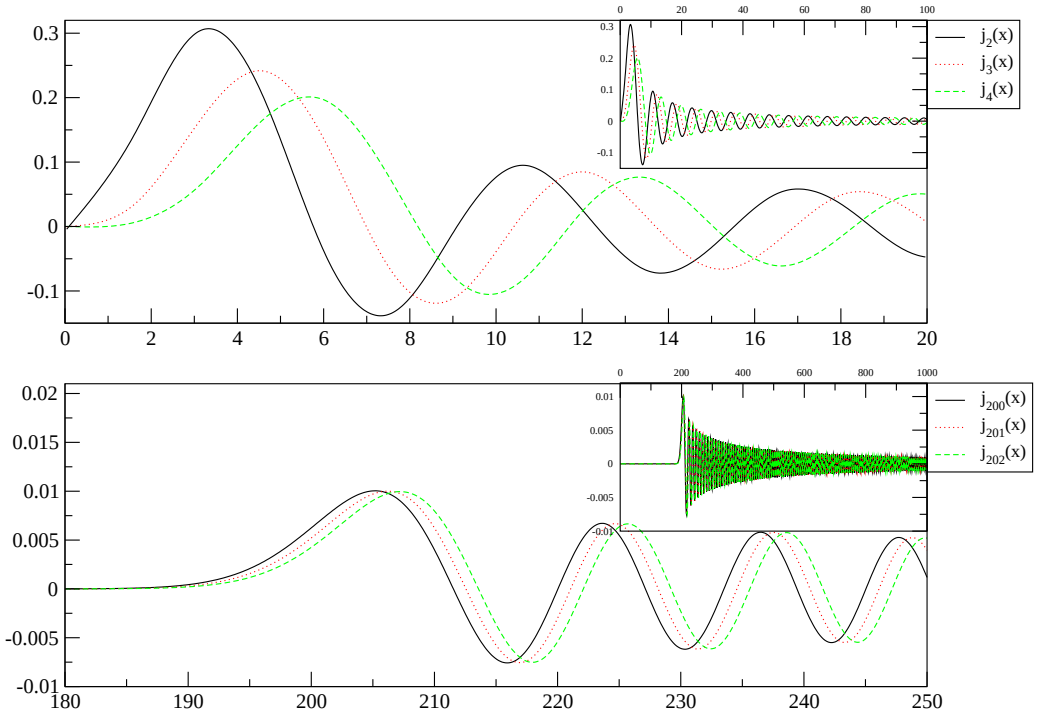

Figure 10: Spherical Bessel functions $j_\ell(x)$ for $\ell = 2$, 3, 4, 200, 201, and 202. Note how the first and largest peak is near $x = \ell$ (but to be precise, at a slightly larger value). Figure by R. Keskitalo.

12.3 Important Distance Scales on the Last Scattering Surface

12.3.1 Angular Diameter Distance to Last Scattering

In Chapter 4 we derived the formula for the comoving distance to redshift z,

$$d^c(z) = H_0^{-1} \int_{\frac{1}{1+z}}^{1} \frac{dx}{\sqrt{\Omega_0(x-x^2) - \Omega_\Lambda(x-x^4) + x^2}} \tag{27}$$

(where we have approximated $\Omega_0 \approx \Omega_m + \Omega_\Lambda$) and the corresponding comoving angular diameter distance

$$d_A^c(z) = a_0 S_K\left(\frac{d_c(z)}{a_0}\right), \tag{28}$$

where

$$S_K(x) \equiv \begin{cases} K^{-1/2}\sin(K^{1/2}x)\,, & K>0 \\ x\,, & K=0 \\ |K|^{-1/2}\sinh(|K|^{1/2}x)\,, & K<0\,. \end{cases} \tag{29}$$

We also define

$$S_k(\chi) \equiv \begin{cases} \sin(\chi)\,, & k=1 \\ \chi\,, & k=0 \\ \sinh(\chi)\,, & k=-1\,. \end{cases} \tag{30}$$

For the flat universe ($K = k = 0$, $\Omega_0 = 1$), the comoving angular diameter distance is equal to the comoving distance,

$$d_A^c(z) = d^c(z) \qquad (K=0)\,. \tag{31}$$

For the open ($K < 0$, $\Omega_0 < 1$) and closed ($K > 0$, $\Omega_0 > 1$) cases we can write Eq. (28) as

$$\begin{aligned} d_A^c(z) &= \frac{H_0^{-1}}{\sqrt{|\Omega_0 - 1|}}\, S_k\left(\frac{\sqrt{|\Omega_0-1|}}{H_0^{-1}}\, d^c(z)\right) \\ &= H_0^{-1}\frac{1}{\sqrt{|\Omega_0-1|}}\, S_k\left(\sqrt{|\Omega_0-1|}\int_{\frac{1}{1+z}}^{1}\frac{dx}{\sqrt{\Omega_0(x-x^2)-\Omega_\Lambda(x-x^4)+x^2}}\right). \end{aligned} \tag{32}$$

Thus $d_A^c(z) \propto H_0^{-1}$, and has some more complicated dependence on Ω_0 and Ω_Λ (or on Ω_m and Ω_Λ).

We are now interested in the distance to the last scattering sphere, i.e., $d_A^c(z_{\rm dec})$, where $1 + z_{\rm dec} \approx 1100$.

For the simplest case, $\Omega_\Lambda = 0$, $\Omega_m = 1$, the integral gives

$$d_A^c(z_{\rm dec}) = H_0^{-1}\int_{\frac{1}{1+z}}^{1}\frac{dx}{\sqrt{x}} = 2H_0^{-1}\left(1 - \frac{1}{\sqrt{1+z_{\rm dec}}}\right) = 1.94H_0^{-1} \approx 2H_0^{-1}\,, \tag{33}$$

where the last approximation corresponds to ignoring the contribution from the lower limit.

We shall consider two more general cases, of which the above is a special case of both:

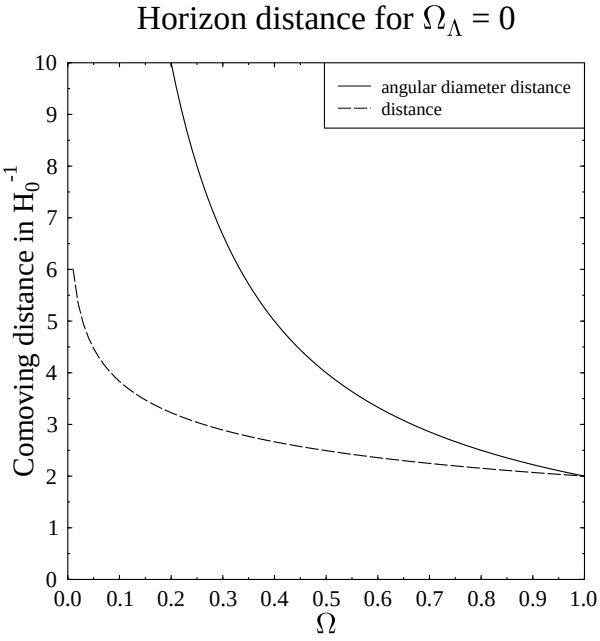

Figure 11: The comoving distance $d^c(z=\infty)$ (dashed) and the comoving angular diameter distance $d_A^c(z=\infty)$ (solid) to the horizon in matter-only open universe. The vertical axis is the distance in units of Hubble distance H_0^{-1} and the horizontal axis is the density parameter $\Omega_0 = \Omega_m$. The distances to last scattering, $d^c(z_{\rm dec})$ and $d_A^c(z_{\rm dec})$ are a few per cent less.

a) Open universe with no dark energy: $\Omega_\Lambda = 0$ and $\Omega_m = \Omega_0 < 1$. Now the integral gives

$$\begin{aligned} d_A^c(z_{\rm dec}) &= \frac{H_0^{-1}}{\sqrt{1-\Omega_m}} \sinh\left(\sqrt{1-\Omega_m}\int_{\frac{1}{1+z}}^1 \frac{dx}{\sqrt{(1-\Omega_m)x^2+\Omega_m x}}\right) \\ &= \frac{H_0^{-1}}{\sqrt{1-\Omega_m}} \sinh\left(\int_{\frac{1}{1+z}}^1 \frac{dx}{\sqrt{x^2+\frac{\Omega_m}{1-\Omega_m}x}}\right) \\ &= \frac{H_0^{-1}}{\sqrt{1-\Omega_m}} \sinh\left(2\,\mathrm{arsinh}\sqrt{\frac{1-\Omega_m}{\Omega_m}} - 2\,\mathrm{arsinh}\sqrt{\frac{1-\Omega_m}{\Omega_m}\frac{1}{1+z_{\rm dec}}}\right) \\ &\approx \frac{H_0^{-1}}{\sqrt{1-\Omega_m}} \sinh\left(2\,\mathrm{arsinh}\sqrt{\frac{1-\Omega_m}{\Omega_m}}\right) = 2\frac{H_0^{-1}}{\Omega_m}\,, \end{aligned} \tag{34}$$

where again the approximation ignores the contribution from the lower limit (i.e., it actually gives the angular diameter distance to the horizon, $d_A^c(z=\infty)$, in a model where we ignore the effect of other energy density components besides matter). In the last step we used $\sinh 2x = 2\sinh x\cosh x = 2\sinh x\sqrt{1+\sinh^2 x}$. We show this result (together with $d^c(z=\infty)$) in Fig.11.

b) Flat universe with vacuum energy, $\Omega_\Lambda + \Omega_m = 1$. Here the integral does not give an elementary function, but a reasonable approximation, which we shall

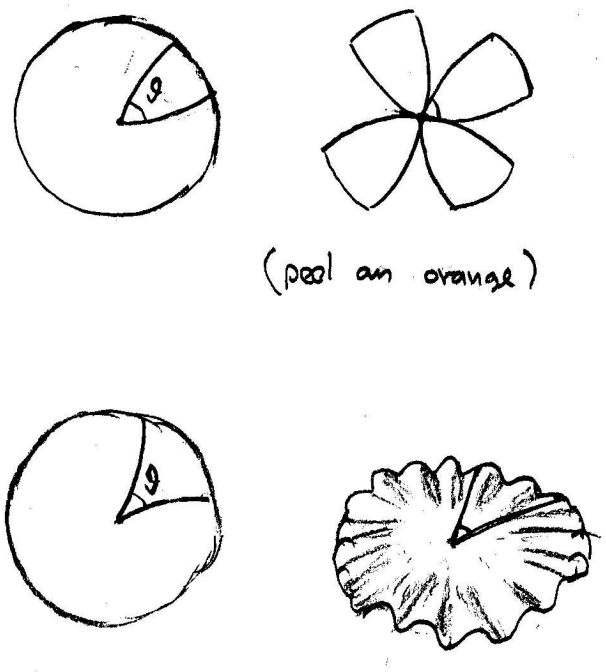

Figure 12: The geometry effect in a closed (top) or an open (bottom) universe affects the angle at which we see a structure of given size at the last scattering surface, and thus its angular diameter distance.

use in the following, is

$$d_A^c(z_{\rm dec}) = d^c(z_{\rm dec}) \approx \frac{2}{\Omega_m^{0.4}} H_0^{-1}\,. \tag{35}$$

The comoving distance $d_c(z_{\rm dec})$ depends on the expansion history of the universe. For one, the longer it takes for the universe to cool from $T_{\rm dec}$ to T_0 (i.e., to expand by the factor $1+z_{\rm dec}$), the longer distance the photons have time to travel. The longer part of this time is spent at small values of the scale factor, the bigger boost this distance gets from converting it to a comoving distance. For open/closed universes the angular diameter distance gets an additional effect from the geometry of the universe, which acts like a "lens" to make the distant CMB pattern at the last scattering sphere to look smaller or larger (see Fig. 12).

12.3.2 Hubble Scale and the Matter-Radiation Equality Scale

We have learned that subhorizon ($k \gg \mathcal{H}$) and superhorizon ($k \ll \mathcal{H}$) scales behave differently. Thus we want to know which of the structures we see on the last scattering surface are subhorizon and which are superhorizon. For that we need to know the comoving Hubble scale $\mathcal{H}$ at $t_{\rm dec}$.

We shall make the approximation that the universe was (completely) matter-dominated at $t_{\rm dec}$, i.e., we ignore the radiation contribution to the Friedmann equation at $t_{\rm dec}$. This is not a terribly good approximation, since

$$\frac{\rho_m(t_{\rm dec})}{\rho_r(t_{\rm dec})} = 21.8\,\Omega_m h^2 = 2.99\,, \tag{36}$$

where the last number is for the WMAP 5-year (WMAP5) value $\Omega_m h^2 = 0.137$ [3]. The curvature and dark energy contributions are negligible at $t_{\rm dec}$. Thus we have

$$H_{\rm dec}^2 \approx \frac{8\pi G}{3}\rho_m = \Omega_m H_0^2 (1+z_{\rm dec})^3 \tag{37}$$

and we get for the comoving Hubble scale

$$k_{\rm dec}^{-1} \equiv \mathcal{H}_{\rm dec}^{-1} = (1+z_{\rm dec}) H_{\rm dec}^{-1} = (1+z_{\rm dec})^{-1/2} \frac{H_0^{-1}}{\sqrt{\Omega_m}} = \frac{1}{\sqrt{\Omega_m}}\, 90 h^{-1}{\rm Mpc}\,. \tag{38}$$

(using $1 + z_{\rm dec} = 1100$). The scale which is just entering at $t = t_{\rm dec}$ is thus

$$k_{\rm dec} = \mathcal{H}_{\rm dec} = (1+z_{\rm dec})^{1/2} \sqrt{\Omega_m} H_0 \tag{39}$$

and the corresponding multipole number on the last scattering sphere is

$$\ell_H \;\equiv\; k_{\rm dec} d_A^c \;=\; (1+z_{\rm dec})^{1/2} \sqrt{\Omega_m} \times \left\{ \begin{array}{lll} 2/\Omega_m & = & 66.3\;\Omega_m^{-0.5} \quad (\Omega_\Lambda = 0) \\ 2/\Omega_m^{0.4} & \approx & 66.3\;\Omega_m^{0.1} \quad (\Omega_0 = 1) \end{array} \right. \tag{40}$$

The angle subtended by a half-wavelength π/k of this mode on the last scattering sphere is

$$\vartheta_H \equiv \frac{\pi}{\ell_H} = \frac{180^\circ}{\ell_H} = \left\{ \begin{array}{l} 2.7^\circ \Omega_m^{0.5} \\ 2.7^\circ \Omega_m^{-0.1} \end{array} \right. \tag{41}$$

For $\Omega_m \sim 0.3$, $\Omega_\Lambda \sim 0.7$ this is $\sim 3^\circ$.

Another important scale is $k_{\rm eq}$, the scale which enters at the time of matter-radiation equality $t_{\rm eq}$, since the transfer function $T(k)$ is bent at that point. Perturbations for scales $k \ll k_{\rm eq}$ maintain essentially their primordial spectrum, whereas scales $k \gg k_{\rm eq}$ have lost relative power between their horizon entry and $t_{\rm eq}$. This scale is

$$k_{\rm eq}^{-1} = \mathcal{H}_{\rm eq}^{-1} \sim 14 \Omega_m^{-1} h^{-2}\ {\rm Mpc} = 4.7 \times 10^{-3} \Omega_m^{-1} h^{-1} H_0^{-1} \tag{42}$$

and the corresponding multipole number of these scales seen on the last scattering sphere is

$$l_{\rm eq} = k_{\rm eq} d_A^c = 214 \Omega_m h \times \left\{ \begin{array}{lll} 2/\Omega_m & = & 430h \quad (\Omega_\Lambda = 0) \\ 2/\Omega_m^{0.4} & \approx & 430h\;\Omega_m^{0.6} \quad (\Omega_0 = 1) \end{array} \right. \tag{43}$$

12.4 CMB Anisotropy from Perturbation Theory

We began this chapter with the observation, Eq. (1), that the CMB temperature anisotropy is a sum of two parts,

$$\left(\frac{\delta T}{T}\right)_{\rm obs} = \left(\frac{\delta T}{T}\right)_{\rm intr} + \left(\frac{\delta T}{T}\right)_{\rm jour}, \tag{44}$$

and that this separation is gauge dependent. We shall consider this in the conformal-Newtonian gauge, since the second part, $\left(\frac{\delta T}{T}\right)_{\rm jour}$, the integrated redshift perturbation along the line of sight, is easiest to calculate in this gauge. (However, we won't do the calculation here.)

The result of this calculation is

$$\begin{aligned}\left(\frac{\delta T}{T}\right)_{\rm jour} &= -\int d\Phi + \int (\dot\Phi + \dot\Psi) dt + \boldsymbol{v}_{\rm obs}\cdot\hat{\boldsymbol{n}} \\ &= \Phi(t_{\rm dec},\boldsymbol{x}_{\rm ls}) - \Phi(t_0,\boldsymbol{0}) + \int (\dot\Phi + \dot\Psi) dt + \boldsymbol{v}_{\rm obs}\cdot\hat{\boldsymbol{n}} \\ &\overset{\Psi\approx\Phi}{=} \Phi(t_{\rm dec},\boldsymbol{x}_{\rm ls}) - \Phi(t_0,\boldsymbol{0}) + 2\int \dot\Phi dt + \boldsymbol{v}_{\rm obs}\cdot\hat{\boldsymbol{n}}\end{aligned} \tag{45}$$

where the integral is from $(t_{\rm dec},\boldsymbol{x}_{\rm ls})$ to $(t_0,\boldsymbol{0})$ along the path of the photon (a null geodesic). The origin $\boldsymbol{0}$ is located where the observer is. The last term, $\boldsymbol{v}_{\rm obs}\cdot\hat{\boldsymbol{n}}$ is the Doppler effect from observer motion (assumed nonrelativistic), $\boldsymbol{v}_{\rm obs}$ being the observer velocity and $\hat{\boldsymbol{n}}$ the direction we are looking at. The ${}_{\rm ls}$ in $\boldsymbol{x}_{\rm ls}$ is just to remind us that $\boldsymbol{x}$ lies somewhere on the last scattering sphere. In the matter-dominated universe the Newtonian potential remains constant in time, $\dot\Phi = 0$, so we get a contribution from the integral only from epochs when radiation or dark energy contributions to the total energy density, or the effect of curvature, cannot be ignored. We can understand the above result as follows. If the potential is constant in time, the blueshift the photon acquires when falling into a potential well is canceled by the redshift from climbing up the well. Thus the net redshift/blueshift caused by gravitational potential perturbations is just the difference between the values of Φ at the beginning and in the end. However, if the potential is changing while the photon is traversing the well, this cancelation is not exact, and we get the integral term to account for this effect.

The value of the potential perturbation at the observing site, $\Phi(t_0,\boldsymbol{0})$ is the same for photons coming from all directions. Thus it does not contribute to the observed anisotropy. It just produces an overall shift in the observed average temperature. This is included in the observed value $T_0 = 2.725$ K, and there is no way for us to separate it from the "correct" unperturbed value. Thus we can ignore it. The observer motion $\boldsymbol{v}_{\rm obs}$ causes a dipole ($\ell = 1$) pattern in the CMB anisotropy, and likewise, there is no way for us to separate from it the cosmological dipole on the last scattering sphere. Therefore the dipole is usually removed from the CMB map before analyzing it for cosmological purposes. Accordingly, we shall ignore this term also, and our final result is

$$\left(\frac{\delta T}{T}\right)_{\rm jour} = \Phi(t_{\rm dec},\boldsymbol{x}_{\rm ls}) + 2\int \dot\Phi dt\,. \tag{46}$$

The other part, $\left(\frac{\delta T}{T}\right)_{\rm intr}$, comes from the local temperature perturbation at $t = t_{\rm dec}$ and the Doppler effect, $-\boldsymbol{v}\cdot\hat{\boldsymbol{n}}$, from the local (baryon+photon) fluid motion at that time. Since

$$\rho_\gamma = \frac{\pi^2}{15}T^4\,, \tag{47}$$

the local temperature perturbation is directly related to the relative perturbation in the photon energy density,

$$\left(\frac{\delta T}{T}\right)_{\rm intr} = \frac{1}{4}\delta_\gamma - \boldsymbol{v}\cdot\hat{\boldsymbol{n}}\,. \tag{48}$$

We can now write the observed temperature anisotropy as

$$\left(\frac{\delta T}{T}\right)_{\rm obs} = \frac{1}{4}\delta_\gamma^N - \boldsymbol{v}^N\cdot\hat{\boldsymbol{n}} + \Phi(t_{\rm dec},\boldsymbol{x}_{\rm ls}) + 2\int\dot{\Phi}dt\,. \tag{49}$$

(note that both the density perturbation δ_γ and the fluid velocity $\boldsymbol{v}$ are gauge dependent).

To make further progress we now

1. consider adiabatic primordial perturbations only (like we did in Chapter 11), and

2. make the (crude) approximation that the universe is already matter dominated at $t = t_{\rm dec}$.

For adiabatic perturbations there is no perturbation in the ratios of conserved particle number densities. The baryon number and CDM particle number are conserved during recombination, and we can ignore the small effect of recombination on the photon number. (The photons released in recombination are, anyway, not thermalized.) Thus

$$\delta\left(\frac{n_i}{n_\gamma}\right) = 0 \;\Rightarrow\; \frac{\delta n_i}{n_i} = \frac{\delta n_\gamma}{n_\gamma} = 3\left(\frac{\delta T}{T}\right)_{\rm intr}\,, \tag{50}$$

(since $n_\gamma \propto T^3$) where i refers to baryons or CDM particles, i.e., to any matter particles we have. Since $\rho_i = m_i n_i$, we have

$$\delta_b = \delta_c \equiv \delta_m = \frac{3}{4}\delta_\gamma\,. \tag{51}$$

The perturbations stay adiabatic only at superhorizon scales. Once the perturbation has entered horizon, different physics can begin to act on different matter components, so that the adiabatic relation between their density perturbations is broken. In particular, the baryon+photon perturbation is affected by photon pressure, which will damp their growth and cause them to oscillate, whereas the CDM perturbation is unaffected and keeps growing. Since the baryon and photon components see the same pressure they still evolve together and maintain their adiabatic relation until photon decoupling. Thus, after horizon entry, but before decoupling,

$$\delta_c \neq \delta_b = \frac{3}{4}\delta_\gamma\,. \tag{52}$$

At decoupling, the equality holds for scales larger than the photon mean free path at $t_{\rm dec}$.

After decoupling, this connection between the photons and baryons is broken, and the baryon density perturbation begins to approach the CDM density perturbation,

$$\delta_c \leftarrow \delta_b \neq \frac{3}{4}\delta_\gamma \,. \tag{53}$$

We shall return to these issues as we discuss the shorter scales in Sections 12.6 and 12.7. But let us first discuss the scales which are still superhorizon at $t_{\rm dec}$, so that Eq. (51) still applies.

12.5 Large Scales: Sachs–Wolfe Part of the Spectrum

Consider now the scales $k \ll k_{\rm dec}$, or $\ell \ll \ell_H$, which are still superhorizon at decoupling. We can now use the adiabatic condition (51), so that

$$\frac{1}{4}\delta_\gamma = \frac{1}{3}\delta_m \approx \frac{1}{3}\delta \,, \tag{54}$$

where the latter (approximate) equality comes from taking the universe to be matter dominated at $t_{\rm dec}$, so that we can identify $\delta \approx \delta_m$. For these scales the Doppler effect from fluid motion is subdominant, and we can ignore it (roughly speaking, the fluid is set into motion by gradients in the pressure and gravitational potential, but the fluid only notices them when the scale is approaching the horizon).

Thus Eq. (49) becomes

$$\left(\frac{\delta T}{T}\right)_{\rm obs} = \frac{1}{3}\delta^N + \Phi(t_{\rm dec}, \boldsymbol{x}_{\rm ls}) + 2\int \dot{\Phi} dt \,. \tag{55}$$

The Newtonian relation

$$\delta = \frac{1}{4\pi G\bar{\rho}}\left(\frac{a_0}{a}\right)^2 \nabla^2\Phi = \frac{2}{3}\left(\frac{a_0}{aH}\right)^2 \nabla^2\Phi$$

(here ∇ is with respect to the comoving coordinates, hence the a_0/a) or

$$\delta_{\boldsymbol{k}} = -\frac{2}{3}\left(\frac{k}{\mathcal{H}}\right)^2 \Phi_{\boldsymbol{k}}$$

does not hold at superhorizon scales (where δ is gauge dependent). A GR calculation using the Newtonian gauge gives the result

$$\delta^N_{\boldsymbol{k}} = -\left[2 + \frac{2}{3}\left(\frac{k}{\mathcal{H}}\right)^2\right]\Phi_{\boldsymbol{k}} \tag{56}$$

for perturbations in a matter-dominated universe. Thus for superhorizon scales we can approximate

$$\delta^N \approx -2\Phi \tag{57}$$

and Eq. (55) becomes

$$\left(\frac{\delta T}{T}\right)_{\rm obs} = -\frac{2}{3}\Phi(t_{\rm dec},\boldsymbol{x}_{\rm ls}) + \Phi(t_{\rm dec},\boldsymbol{x}_{\rm ls}) + 2\int \dot{\Phi} dt$$
$$= \frac{1}{3}\Phi(t_{\rm dec},\boldsymbol{x}_{\rm ls}) + 2\int \dot{\Phi} dt\,. \qquad (58)$$

This explains the "mysterious" factor 1/3 in this relation between the potential Φ and the temperature perturbation.

This result is called the *Sachs–Wolfe effect*. The first part, $\frac{1}{3}\Phi(t_{\rm dec},\boldsymbol{x}_{\rm ls})$, is called the *ordinary* Sachs–Wolfe effect, and the second part, $2\int\dot{\Phi}dt$, the *integrated Sachs-Wolfe effect* (ISW), since it involves integrating along the line of sight. Note that the approximation of matter domination at $t = t_{\rm dec}$, making $\dot{\Phi} = 0$, does not eliminate the ISW, since it only applies to the "early part" of the integral. At times closer to t_0, dark energy may (and apparently does) become important, causing Φ to evolve again. This ISW caused by dark energy (or curvature of the background universe, if $k \neq 0$) is called the *late Sachs–Wolfe effect* (LSW) and it shows up as a rise in the smallest ℓ of the angular power spectrum C_ℓ. Correspondingly, the contribution to the ISW from the evolution of Φ near $t_{\rm dec}$ due to the radiation contribution to the expansion law (which we ignored in our approximation) is called the *early Sachs–Wolfe effect* (ESW). The ESW shows up as a rise in C_ℓ for larger ℓ, near ℓ_H.

We shall now forget for a while the ISW, which for $\ell \ll \ell_H$ is expected to be smaller than the ordinary Sachs–Wolfe effect.

12.5.1 Angular power spectrum from the ordinary Sachs–Wolfe effect

We now calculate the contribution from the ordinary Sachs–Wolfe effect,

$$\left(\frac{\delta T}{T}\right)_{\rm SW} = \frac{1}{3}\Phi(t_{\rm dec},\boldsymbol{x}_{\rm ls})\,, \qquad (59)$$

to the angular power spectrum C_ℓ. This is the dominant effect for $\ell \ll \ell_H$.

Since Φ is evaluated at the last scattering sphere, we have, from Eq. (23),

$$a_{\ell m} = 4\pi i^\ell \sum_{\boldsymbol{k}} \frac{1}{3}\Phi_{\boldsymbol{k}} j_\ell(kx) Y^*_{\ell m}(\hat{\boldsymbol{k}})\,, \qquad (60)$$

In the matter-dominated epoch,

$$\Phi = -\frac{3}{5}\mathcal{R}\,, \qquad (61)$$

so that we have

$$a_{\ell m} = -\frac{4\pi}{5} i^\ell \sum_{\boldsymbol{k}} \mathcal{R}_{\boldsymbol{k}} j_\ell(kx) Y^*_{\ell m}(\hat{\boldsymbol{k}})\,. \qquad (62)$$

The coefficient $a_{\ell m}$ is thus a linear combination of the independent random variables $\mathcal{R}_{\boldsymbol{k}}$, i.e., it is of the form

$$\sum_{\boldsymbol{k}} b_{\boldsymbol{k}} \mathcal{R}_{\boldsymbol{k}}\,, \qquad (63)$$

For any such linear combination, the expectation value of its absolute value squared is

$$\left\langle \left| \sum_{\boldsymbol{k}} b_{\boldsymbol{k}} \mathcal{R}_{\boldsymbol{k}} \right|^2 \right\rangle = \sum_{\boldsymbol{k}} \sum_{\boldsymbol{k}'} b_{\boldsymbol{k}} b^*_{\boldsymbol{k}'} \left\langle \mathcal{R}_{\boldsymbol{k}} \mathcal{R}^*_{\boldsymbol{k}'} \right\rangle = \left(\frac{2\pi}{L} \right)^3 \sum_{\boldsymbol{k}} \frac{1}{4\pi k^3} \mathcal{P}_{\mathcal{R}}(k) \left| b_{\boldsymbol{k}} \right|^2 , \tag{64}$$

where we used

$$\left\langle \mathcal{R}_{\boldsymbol{k}} \mathcal{R}^*_{\boldsymbol{k}'} \right\rangle = \delta_{\boldsymbol{k}\boldsymbol{k}'} \left(\frac{2\pi}{L} \right)^3 \frac{1}{4\pi k^3} \mathcal{P}_{\mathcal{R}}(k) \tag{65}$$

(the independence of the random variables $\mathcal{R}_{\boldsymbol{k}}$ and the definition of the power spectrum $\mathcal{P}(k)$).

Thus

$$\begin{aligned} C_\ell &\equiv \frac{1}{2\ell+1} \sum_m \langle |a_{\ell m}|^2 \rangle \\ &= \frac{16\pi^2}{25} \frac{1}{2\ell+1} \sum_m \left(\frac{2\pi}{L} \right)^3 \sum_{\boldsymbol{k}} \frac{1}{4\pi k^3} \mathcal{P}_{\mathcal{R}}(k) j_\ell(kx)^2 \left| Y^*_{\ell m}(\hat{\boldsymbol{k}}) \right|^2 \\ &= \frac{1}{25} \left(\frac{2\pi}{L} \right)^3 \sum_{\boldsymbol{k}} \frac{1}{k^3} \mathcal{P}_{\mathcal{R}}(k) j_\ell(kx)^2 . \end{aligned} \tag{66}$$

(Although all $\langle |a_{\ell m}|^2 \rangle$ are equal for the same ℓ, we used the sum over m, so that we could use Eq. (5).) Replacing the sum with an integral, we get

$$\begin{aligned} C_\ell &= \frac{1}{25} \int \frac{d^3k}{k^3} \mathcal{P}_{\mathcal{R}}(k) j_\ell(kx)^2 \\ &= \frac{4\pi}{25} \int_0^\infty \frac{dk}{k} \mathcal{P}_{\mathcal{R}}(k) j_\ell(kx)^2 , \end{aligned} \tag{67}$$

the final result for an arbitrary primordial power spectrum $\mathcal{P}_{\mathcal{R}}(k)$.

The integral can be done for a power-law power spectrum, $\mathcal{P}(k) = A^2 k^{n-1}$. In particular, for a scale-invariant ($n = 1$) primordial power spectrum,

$$\mathcal{P}_{\mathcal{R}}(k) = \text{const.} = A^2 , \tag{68}$$

we have

$$C_\ell = A^2 \frac{4\pi}{25} \int_0^\infty \frac{dk}{k} j_\ell(kx)^2 = \frac{A^2}{25} \frac{2\pi}{\ell(\ell+1)} , \tag{69}$$

since

$$\int_0^\infty \frac{dk}{k} j_\ell(kx)^2 = \frac{1}{2\ell(\ell+1)} . \tag{70}$$

We can write this as

$$\frac{\ell(\ell+1)}{2\pi} C_\ell = \frac{A^2}{25} = \text{const. (independent of } \ell) \tag{71}$$

This is the reason why the angular power spectrum is customarily plotted as $\ell(\ell+1)C_\ell/2\pi$; it makes the Sachs–Wolfe part of the C_ℓ flat for a scale-invariant primordial power spectrum $\mathcal{P}_{\mathcal{R}}(k)$.

Present data is consistent with an almost scale-invariant primordial power spectrum (actually it favors a small red tilt, $n < 1$). The constant A can be determined from the Sachs–Wolfe part of the observed $\widehat{C}_\ell$. The COBE satellite saw only up to about $\ell = 25$, so the COBE data is completely in the Sachs–Wolfe region. The COBE data has

$$\frac{\ell(\ell+1)}{2\pi}\widehat{C}_\ell \sim 10^{-10} \tag{72}$$

on the average. This gives the amplitude of the primordial power spectrum as

$$\mathcal{P}_{\mathcal{R}}(k) = A^2 \sim 25 \times 10^{-10} = \left(5 \times 10^{-5}\right)^2 . \tag{73}$$

We already used this result in Chapter 11 as a constraint on the energy scale of inflation.

12.6 Acoustic Oscillations

Consider now the scales $k \gg k_{\rm dec}$, or $\ell \gg \ell_H$, which are subhorizon at decoupling. The observed temperature anisotropy is, from Eq. (49)

$$\left(\frac{\delta T}{T}\right)_{\rm obs} = \frac{1}{4}\delta_\gamma(t_{\rm dec}, \boldsymbol{x}_{\rm ls}) + \Phi(t_{\rm dec}, \boldsymbol{x}_{\rm ls}) - \boldsymbol{v}\cdot\hat{\boldsymbol{n}}(t_{\rm dec}, \boldsymbol{x}_{\rm ls}) + 2\int \dot{\Phi} dt\,. \tag{74}$$

Since we are considering subhorizon scales, we dropped the reference to the Newtonian gauge. We shall concentrate on the three first terms, which correspond to the situation at the point $(t_{\rm dec}, \boldsymbol{x}_{\rm ls})$ we are looking at on the last scattering sphere.

Before decoupling the photons are coupled to the baryons. The perturbations in the baryon-photon fluid are oscillating, whereas CDM perturbations grow (slowly during the radiation-dominated epoch, and then faster during the matter-dominated epoch). Therefore CDM perturbations begin to dominate the total density perturbation $\delta\rho$ and thus also Φ already before the universe becomes matter dominated, and CDM begins to dominate the background energy density. Thus we can make the approximation that Φ is given by the CDM perturbation. The baryon-photon fluid oscillates in these potential wells caused by the CDM. The potential Φ evolves at first but then becomes constant as the universe becomes matter dominated.

We shall not attempt an exact calculation of the $\delta_{b\gamma}$ oscillations in the expanding universe. One reason is that $\rho_{b\gamma}$ is a relativistic fluid, and we have derived the perturbation equations for a nonrelativistic fluid only. From Sec. 11.1.7 we have that the nonrelativistic perturbation equation for a fluid component i is

$$\ddot{\delta}_{\boldsymbol{k}i} + 2H\dot{\delta}_{\boldsymbol{k}i} = -\left(\frac{a_0}{a}\right)^2 k^2 \left(\frac{\delta p_{\boldsymbol{k}i}}{\bar{\rho}_i} + \Phi_{\boldsymbol{k}}\right) . \tag{75}$$

The generalization of the (subhorizon) perturbation equations to the case of a relativistic fluid is considerably easier if we ignore the expansion of the universe. Then Eq. (75) becomes

$$\ddot{\delta}_{\boldsymbol{k}i} + k^2 \left(\frac{\delta p_{\boldsymbol{k}i}}{\bar{\rho}_i} + \Phi_{\boldsymbol{k}}\right) = 0\,. \tag{76}$$

According to GR, the density of "passive gravitational mass" is $\rho + p = (1+w)\rho$, not just ρ as in Newtonian gravity. Therefore the force on a fluid element of the fluid

component i is proportional to $(\rho_i + p_i)\nabla\Phi = (1 + w_i)\rho_i\nabla\Phi$ instead of just $\rho_i\nabla\Phi$, and Eq. (76) generalizes to the case of a relativistic fluid as[4]

$$\ddot{\delta}_{\boldsymbol{k}i} + k^2 \left[\frac{\delta p_{\boldsymbol{k}i}}{\bar{\rho}_i} + (1 + w_i)\Phi_{\boldsymbol{k}} \right] = 0 \,. \tag{77}$$

In the present application the fluid component ρ_i is the baryon-photon fluid $\rho_{b\gamma}$ and the gravitational potential Φ is caused by the CDM. Before decoupling, the adiabatic relation $\delta_b = \frac{3}{4}\delta_\gamma$ still holds between photons and baryons, and we have the adiabatic relation between pressure and density perturbations,

$$\delta p_{b\gamma} = c_s^2 \delta\rho_{b\gamma} \tag{78}$$

where

$$c_s^2 = \frac{\delta p_{b\gamma}}{\delta\rho_{b\gamma}} \approx \frac{\delta p_\gamma}{\delta\rho_{b\gamma}} = \frac{1}{3}\frac{\delta\rho_\gamma}{\delta\rho_\gamma + \delta\rho_b} = \frac{1}{3}\frac{\bar{\rho}_\gamma\delta_\gamma}{\bar{\rho}_\gamma\delta_\gamma + \bar{\rho}_b\delta_b} = \frac{1}{3}\frac{1}{1 + \frac{3}{4}\frac{\bar{\rho}_b}{\bar{\rho}_\gamma}} \equiv \frac{1}{3}\frac{1}{1+R} \tag{79}$$

gives the speed of sound c_s of the baryon-photon fluid. We defined

$$R \equiv \frac{3}{4}\frac{\bar{\rho}_b}{\bar{\rho}_\gamma} \,. \tag{80}$$

We can now write the perturbation equation (77) for the baryon-photon fluid as

$$\ddot{\delta}_{b\gamma\boldsymbol{k}} + k^2 \left[c_s^2 \delta_{b\gamma\boldsymbol{k}} + (1 + w_{b\gamma})\Phi_{\boldsymbol{k}} \right] = 0 \,. \tag{81}$$

The equation-of-state parameter for the baryon-photon fluid is

$$w_{b\gamma} \equiv \frac{\bar{p}_{b\gamma}}{\bar{\rho}_{b\gamma}} = \frac{\frac{1}{3}\bar{\rho}_\gamma}{\bar{\rho}_\gamma + \bar{\rho}_b} = \frac{1}{3}\frac{1}{1 + \frac{4}{3}R} \,, \tag{82}$$

so that

$$1 + w_{b\gamma} = \frac{\frac{4}{3}(1+R)}{1 + \frac{4}{3}R} \tag{83}$$

and we can write Eq. (81) as

$$\ddot{\delta}_{b\gamma\boldsymbol{k}} + k^2 \left[\frac{1}{3}\frac{1}{1+R}\delta_{b\gamma\boldsymbol{k}} + \frac{\frac{4}{3}(1+R)}{1 + \frac{4}{3}R}\Phi_{\boldsymbol{k}} \right] = 0 \,. \tag{84}$$

For the CMB anisotropy we are interested in[5]

$$\Theta_0 \equiv \frac{1}{4}\delta_\gamma \,, \tag{85}$$

which gives the local temperature perturbation, not in $\delta_{b\gamma}$. These two are related by

$$\delta_{b\gamma} = \frac{\delta\rho_{b\gamma}}{\bar{\rho}_{b\gamma}} = \frac{\delta\rho_\gamma + \delta\rho_b}{\bar{\rho}_\gamma + \bar{\rho}_b} = \frac{\bar{\rho}_\gamma\delta_\gamma + \bar{\rho}_b\delta_b}{\bar{\rho}_\gamma + \bar{\rho}_b} = \frac{1+R}{1 + \frac{4}{3}R}\delta_\gamma \,. \tag{86}$$

[4] Actually the derivation is more complicated, since also the density of "inertial mass" is $\rho_i + p_i$ and the energy continuity equation is modified by a work-done-by-pressure term. Anyway, Eq. (77) is the correct result.

[5] The subscript 0 refers to the monopole ($\ell = 0$) of the *local* photon distribution. Likewise, the dipole ($\ell = 1$) of the local photon distribution corresponds to the velocity of the photon fluid, $\Theta_1 \equiv v_\gamma/3$.

Thus we can write Eq. (81) as

$$\ddot{\delta}_{\gamma\boldsymbol{k}} + k^2\left[\frac{1}{3}\frac{1}{1+R}\delta_{\gamma\boldsymbol{k}} + \frac{4}{3}\Phi_{\boldsymbol{k}}\right] = 0\,, \tag{87}$$

or

$$\ddot{\Theta}_{0\boldsymbol{k}} + k^2\left[\frac{1}{3}\frac{1}{1+R}\Theta_{0\boldsymbol{k}} + \frac{1}{3}\Phi_{\boldsymbol{k}}\right] = 0\,, \tag{88}$$

or

$$\ddot{\Theta}_{0\boldsymbol{k}} + c_s^2 k^2\left[\Theta_{0\boldsymbol{k}} + (1+R)\Phi_{\boldsymbol{k}}\right] = 0\,, \tag{89}$$

If we now take R and Φ_k to be constant, this is the harmonic oscillator equation for the quantity $\Theta_{0\boldsymbol{k}} + (1+R)\Phi_{\boldsymbol{k}}$ with the general solution

$$\Theta_{0\boldsymbol{k}} + (1+R)\Phi_{\boldsymbol{k}} = A_{\boldsymbol{k}}\cos c_s kt + B_{\boldsymbol{k}}\sin c_s kt\,, \tag{90}$$

or

$$\Theta_{0\boldsymbol{k}} + \Phi_{\boldsymbol{k}} = -R\Phi_{\boldsymbol{k}} + A_{\boldsymbol{k}}\cos c_s kt + B_{\boldsymbol{k}}\sin c_s kt\,, \tag{91}$$

or

$$\Theta_{0\boldsymbol{k}} = -(1+R)\Phi_{\boldsymbol{k}} + A_{\boldsymbol{k}}\cos c_s kt + B_{\boldsymbol{k}}\sin c_s kt\,. \tag{92}$$

We are interested in the quantity $\Theta_0 + \Phi = \frac{1}{4}\delta_\gamma + \Phi$, called the *effective temperature perturbation*, since this combination appears in Eq. (74). It is the local temperature perturbation minus the redshift photons suffer when climbing from the potential well of the perturbation (negative Φ for a CDM overdensity). We see that this quantity oscillates in time, and the effect of baryons (via R) is to shift the equilibrium point of the oscillation by $-R\Phi_{\boldsymbol{k}}$.

In the preceding we ignored the effect of the expansion of the universe. The expansion affects the preceding in a number of ways. For example, c_s, $w_{b\gamma}$ and R change with time. The potential Φ also evolves, especially at the earlier times when radiation dominates the expansion law. However, the qualitative result of an oscillation of $\Theta_0 + \Phi$, and the shift of its equilibrium point by baryons, remains. The time t in the solution (91) gets replaced by conformal time η, and since c_s changes with time, $c_s\eta$ is replaced by

$$r_s(t) \equiv \int_0^\eta c_s d\eta = a_0\int_0^t \frac{c_s(t)}{a(t)}dt\,. \tag{93}$$

We call this quantity $r_s(t)$ the *sound horizon* at time t, since it represents the comoving distance sound has traveled by time t.

The relative weight of the cosine and sine solutions (i.e., the constants $A_{\boldsymbol{k}}$ and $B_{\boldsymbol{k}}$ in Eq. (90) depends on the initial conditions. Since the perturbations are initially at superhorizon scales, the initial conditions are determined there, and the present discussion does not really apply. However, using the Newtonian gauge superhorizon initial conditions gives the correct qualitative result for the phase of the oscillation.

We had that for adiabatic primordial perturbations, initially $\Phi = -\frac{3}{5}\mathcal{R}$ and $\frac{1}{4}\delta_\gamma^N = -\frac{2}{3}\Phi = \frac{2}{5}\mathcal{R}$, giving us an initial condition $\Theta_0 + \Phi = \frac{1}{3}\Phi = -\frac{1}{5}\mathcal{R} = \text{const.}$ (At these early times $R \ll 1$, so we don't write the $1+R$.) Thus adiabatic primordial perturbations correspond essentially to the cosine solution. (There are affects at the horizon scale which affect the amplitude of the oscillations—the main effect being the decay of Φ as it enters the horizon—so we can't use the preceding discussion to

determine the amplitude, but we get the right result about the initial phase of the $\Theta_0 + \Phi$ oscillations.)

Thus we have that, qualitatively, the effective temperature behaves at subhorizon scales as

$$\Theta_{0\boldsymbol{k}} + (1+R)\Phi_{\boldsymbol{k}} \propto \cos kr_s(t)\,, \tag{94}$$

Consider a region which corresponds to a positive primordial curvature perturbation $\mathcal{R}$. It begins with an initial overdensity (of all components, photons, baryons, CDM and neutrinos), and a negative gravitational potential Φ. For the scales of interest for CMB anisotropy, the potential stays negative, since the CDM begins to dominate the potential early enough and the CDM perturbations do not oscillate, they just grow. The effective temperature perturbation $\Theta_0 + \Phi$, which is the oscillating quantity, begins with a negative value. After half an oscillation period it is at its positive extreme value. This increase of $\Theta_0 + \Phi$ corresponds to an increase in δ_γ; from its initial positive value it has grown to a larger positive value. Thus the oscillation begins by the, already initially overdense, baryon-photon fluid falling deeper into the potential well, and reaching its maximum compression after half a period. After this maximum compression the photon pressure pushes the baryon-photon fluid out from the potential well, and after a full period, the fluid reaches its maximum decompression in the potential well. Since the potential Φ has meanwhile decayed (horizon entry and the resulting potential decay always happens during the first oscillation period, since the sound horizon and the Hubble length are close to each other, as the sound speed is close to the speed of light), the decompression does not bring the $\delta_{b\gamma}$ back to its initial value (which was overdense), but the photon-baryon fluid actually becomes underdense in the potential well (and overdense in the neighboring potential "hill"). And so the oscillation goes on until photon decoupling.

These are standing waves and they are called *acoustic oscillations*. See Fig. 13. Because of the potential decay at horizon entry, the amplitude of the oscillation is larger than Φ, and thus also Θ_0 changes sign in the oscillation.

These oscillations end at photon decoupling, when the photons are liberated. The CMB shows these standing waves as a snapshot[6] at their final moment $t = t_{\rm dec}$.

At photon decoupling we have

$$\Theta_{0\boldsymbol{k}} + (1+R)\Phi_{\boldsymbol{k}} \propto \cos kr_s(t_{\rm dec})\,. \tag{95}$$

At this moment oscillations for scales k which have

$$kr_s(t_{\rm dec}) = m\pi \tag{96}$$

($m = 1, 2, 3, \ldots$) are at their extreme values (maximum compression or maximum decompression). Therefore we see strong structure in the CMB anisotropy at the multipoles

$$\ell = kd_A^c(t_{\rm dec}) = m\pi\frac{d_A^c(t_{\rm dec})}{r_s(t_{\rm dec})} \equiv m\ell_A \tag{97}$$

[6]Actually, photon decoupling takes quite a long time. Therefore this "snapshot" has a rather long "exposure time" causing it to be "blurred". This prevents us from seeing very small scales in the CMB anisotropy.

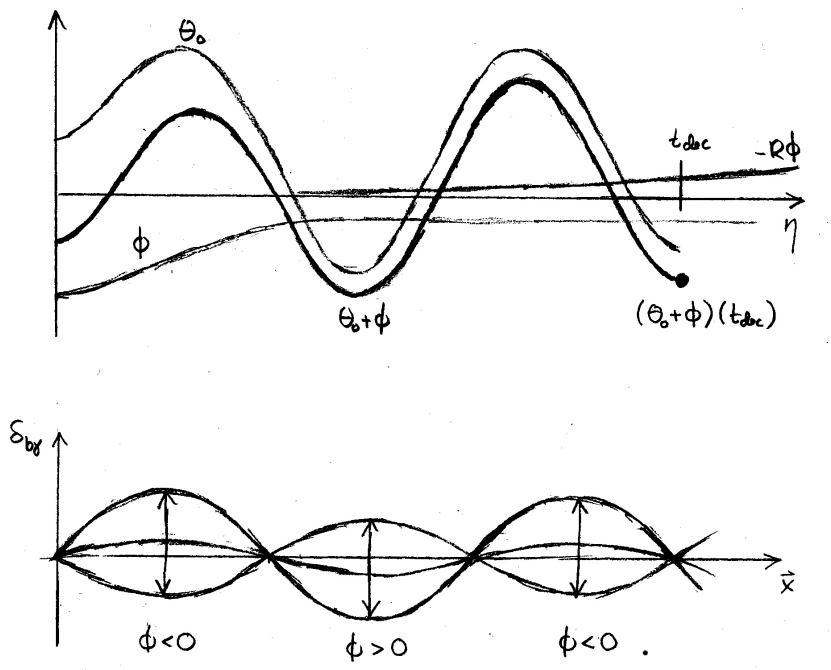

Figure 13: Acoustic oscillations. The top panel shows the time evolution of the Fourier amplitudes $\Theta_{0\boldsymbol{k}}$, $\Phi_{\boldsymbol{k}}$, and the effective temperature $\Theta_{0\boldsymbol{k}} + \Phi_{\boldsymbol{k}}$. The Fourier mode shown corresponds to the fourth acoustic peak of the C_ℓ spectrum. The bottom panel shows $\delta_{b\gamma}(\boldsymbol{x})$ for one Fourier mode as a function of position at various times (maximum compression, equilibrium level, and maximum decompression).

corresponding to these scales. Here

$$\ell_A \equiv \pi \frac{d_A^c(t_{\rm dec})}{r_s(t_{\rm dec})} \equiv \frac{\pi}{\vartheta_s} \tag{98}$$

is the *acoustic scale* in multipole space and

$$\vartheta_s \equiv \frac{r_s(t_{\rm dec})}{d_A^c(t_{\rm dec})} \tag{99}$$

is the *sound horizon angle*, i.e., the angle at which we see the sound horizon on the last scattering surface.

Because of these acoustic oscillations, the CMB angular power spectrum C_ℓ has a structure of *acoustic peaks* at subhorizon scales. The centers of these peaks are located approximately at $\ell_m \approx m\ell_A$. An exact calculation shows that they will actually lie at somewhat smaller ℓ due to a number of effects. The separation of neighboring peaks is closer to ℓ_A, than the positions of the peaks are to $m\ell_A$.

These acoustic oscillations involve motion of the baryon-photon fluid. When the oscillation of one Fourier mode is at its extreme, e.g. at the maximal compression in the potential well, the fluid is momentarily at rest, but then it begins flowing out of the well until the other extreme, the maximal decompression, is reached. Therefore those Fourier modes $\boldsymbol{k}$ which have the maximum effect on the CMB anisotropy via the $\frac{1}{4}\delta_\gamma(t_{\rm dec}, \boldsymbol{x}_{\rm ls}) + \Phi(t_{\rm dec}, \boldsymbol{x}_{\rm ls})$ term (the effective temperature effect) in Eq. (74) have the minimum effect via the $-\boldsymbol{v}\cdot\hat{\boldsymbol{n}}(t_{\rm dec}, \boldsymbol{x}_{\rm ls})$ term (the Doppler effect) and vice versa.

Therefore the Doppler effect also contributes a peak structure to the C_ℓ spectrum, but the peaks are in the locations where the effective temperature contribution has troughs.

The Doppler effect is subdominant to the effective temperature effect, and therefore the peak positions in the C_ℓ spectrum is determined by the effective temperature effect, according to Eq. (97). The Doppler effect just partially fills the troughs between the peaks, weakening the peak structure of C_ℓ. See Fig.16.

Fig. 14 shows the values of the effective temperature perturbation $\Theta_0+\Phi$ (as well as Θ_0 and Φ separately) and the magnitude of the velocity perturbation ($\Theta_1 \sim v/3$) at $t_{\rm dec}$ as a function of the scale k. This is a result of a numerical calculation which includes the effect of the expansion of the universe, but not diffusion damping (Sec. 12.7).

12.7 Diffusion Damping

For small enough scales the effect of photon diffusion and the finite thickness of the last scattering surface ($\sim$ the photon mean free path just before last scattering) smooth out the photon distribution and the CMB anisotropy.

This effect can be characterized by the damping scale $k_D^{-1} \sim$ photon diffusion length $\sim$ geometric mean of the Hubble time and photon mean free path λ_γ. Actually λ_γ is increasing rapidly during recombination, so a calculation of the diffusion scale involves an integral over time which includes this effect.

A calculation, that we shall not do here,[7] gives that photon density and velocity perturbations at scale k are damped at $t_{\rm dec}$ by

$$e^{-k^2/k_D^2}\,, \tag{100}$$

where the diffusion scale is

$$k_D^{-1} \sim \frac{1}{\rm few}\frac{a_0}{a}\sqrt{\frac{\lambda_\gamma(t_{\rm dec})}{H_{\rm dec}}}\,. \tag{101}$$

Accordingly, the C_ℓ spectrum is also damped as

$$e^{-\ell^2/\ell_D^2} \tag{102}$$

where

$$\ell_D \sim k_D d_A^c(t_{\rm dec})\,. \tag{103}$$

For typical values of cosmological parameters $\ell_D \sim 1500$. See Fig. 15 for a result of a numerical calculation with and without diffusion damping.

Of the cosmological parameters, the damping scale is the most strongly dependent on ω_b, since increasing the baryon density shortens the photon mean free path before decoupling. Thus for larger ω_b the damping moves to shorter scales, i.e., ℓ_D becomes larger.

(Of course, decoupling only happens as the photon mean free path becomes comparable to the Hubble length, so one might think that λ_γ at $t_{\rm dec}$ should be independent of ω_b. However there is a distinction here between whether a photon will not scatter again after a particular scattering and what was the mean free path

[7] See, e.g., Dodelson [6], Chapter 8.

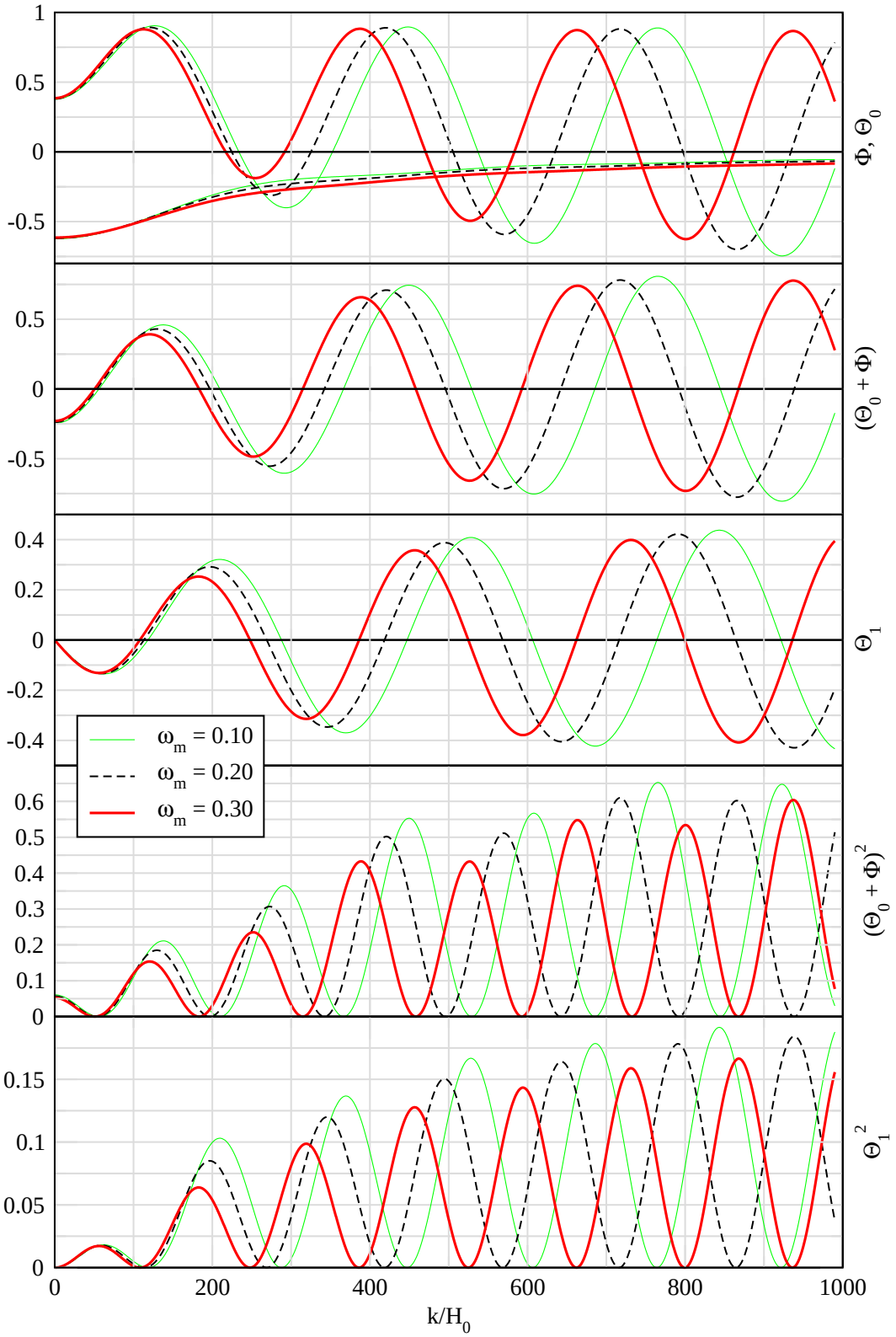

Figure 14: Values of oscillating quantities (normalized to an initial value $\mathcal{R}_{\boldsymbol{k}} = 1$) at the time of decoupling as a function of the scale k, for three different values of ω_m, and for $\omega_b = 0.01$. Θ_1 represents the velocity perturbation. The effect of diffusion damping is neglected. Figure and calculation by R. Keskitalo.

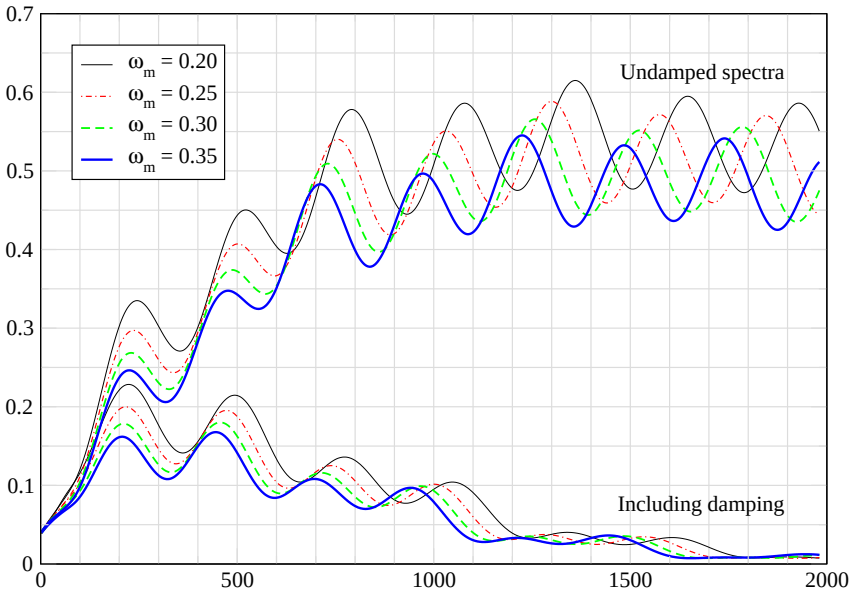

Figure 15: The angular power spectrum C_ℓ, calculated both with and without the effect of diffusion damping. The spectrum is given for four different values of ω_m, with $\omega_b = 0.01$. (This is a rather low value of ω_b, so $\ell_D < 1500$ and damping is quite strong.) Figure and calculation by R. Keskitalo.

between the second-to-last and the last scattering. And k_D depends on an integral over the past history of the photon mean free path, not just the last one. The factor 1/few in Eq.(101) comes from that integration, and actually depends on ω_b. For small ω_b the λ_γ has already become quite large through the slow dilution of the baryon density by the expansion of the universe, and relies less on the fast reduction of free electron density due to recombination. Thus the time evolution of λ_γ before decoupling is different for different ω_b and we get a different diffusion scale.)

12.8 The Complete C_ℓ Spectrum

As we have discussed the CMB anisotropy has three contributions (see Eq. 74), the effective temperature effect,

$$\frac{1}{4}\delta_\gamma(t_{\rm dec}, \boldsymbol{x}_{\rm ls}) + \Phi(t_{\rm dec}, \boldsymbol{x}_{\rm ls})\,, \tag{104}$$

the Doppler effect,

$$-\boldsymbol{v}\cdot\hat{\boldsymbol{n}}(t_{\rm dec}, \boldsymbol{x}_{\rm ls})\,, \tag{105}$$

and the integrated Sachs–Wolfe effect,

$$2\int \dot{\Phi} dt\,. \tag{106}$$

Since the C_ℓ is a quadratic quantity, it also includes cross-terms between these three effects.

The calculation of the full C_ℓ proceeds much as the calculation of just the ordinary Sachs–Wolfe part (which the effective temperature effect becomes at super-horizon scales) in Sec. 12.5.1, but now with the full $\delta T/T$. Since all perturbations are proportional to the primordial perturbations, the C_ℓ spectrum is proportional

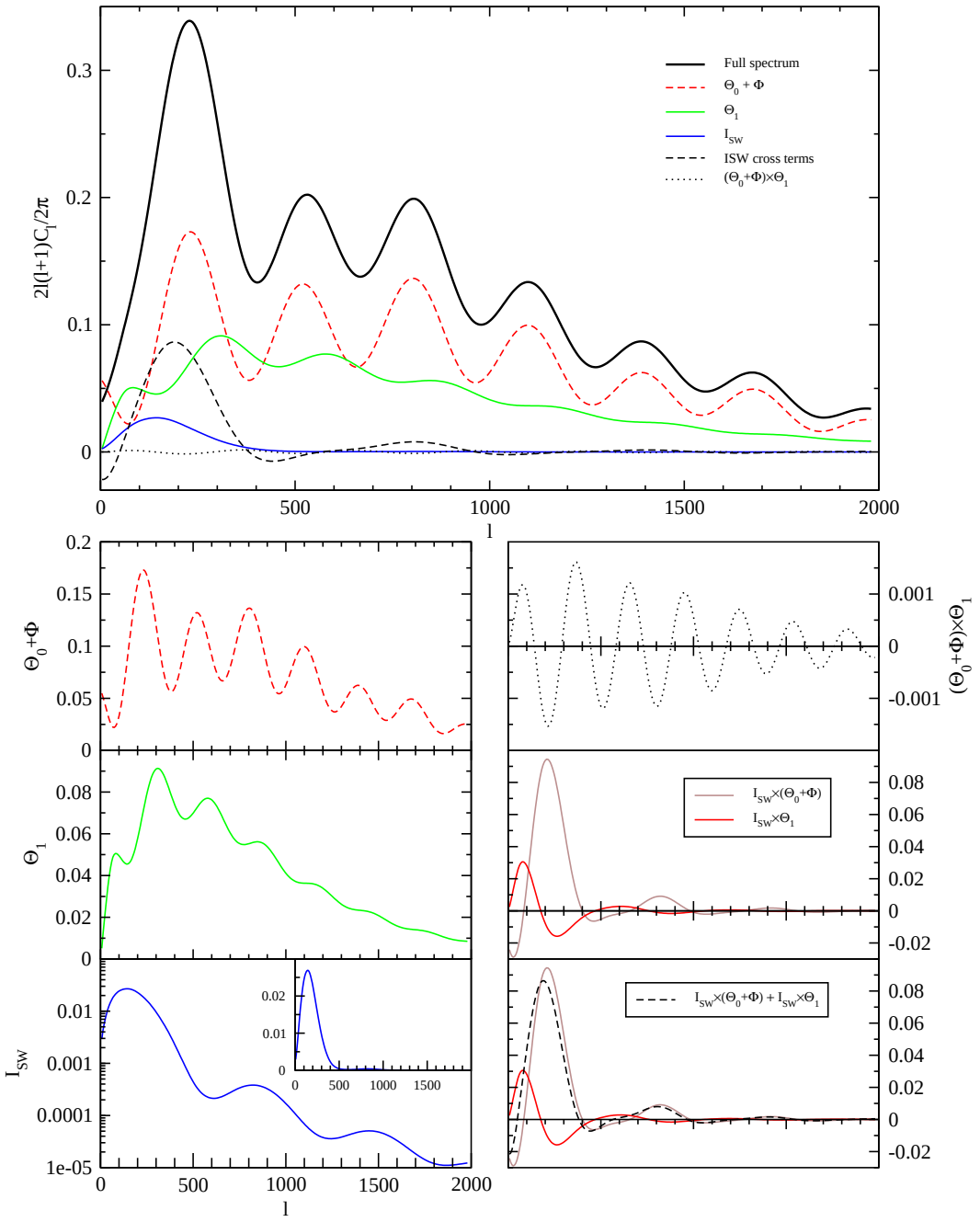

Figure 16: The full C_ℓ spectrum calculated for the cosmological model $\Omega_0 = 1$, $\Omega_\Lambda = 0$, $\omega_m = 0.2$, $\omega_b = 0.03$, $A = 1$, $n = 1$, and the different contributions to it. (The calculation involves some approximations which allow the description of C_ℓ as just a sum of these contributions and is not as accurate as a CMBFAST or CAMB calculation.) Here Θ_1 denotes the Doppler effect. Figure and calculation by R. Keskitalo.

to the primordial perturbation spectrum $\mathcal{P}_\mathcal{R}(k)$ (with integrals over the spherical Bessel functions $j_\ell(kx)$, like in Eq. (67), to get from k to ℓ).

The difference is that instead of the constant proportionality factor $(\delta T/T)_{SW} = -(1/5)\mathcal{R}$, we have a k-dependent proportionality resulting from the evolution (including, e.g., the acoustic oscillations) of the perturbations.

In Fig. 16 we show the full C_ℓ spectrum and the different contributions to it.

Because the Doppler effect and the effective temperature effect are almost completely off-phase, their cross term gives a negligible contribution.

Since the ISW effect is relatively weak, it contributes more via its cross terms with the Doppler effect and effective temperature than directly. The cosmological model used for Fig. 16 has $\Omega_\Lambda = 0$, so there is no late ISW effect (which would contribute at the very lowest ℓ), and the ISW effect shown is the early ISW effect due to radiation contribution to the expansion law. This effect contributes mainly to the first peak and to the left of it, explaining why the first peak is so much higher than the other peaks. It also shifts the first peak position slightly to the left and changes its shape.

12.9 Cosmological Parameters and CMB Anisotropy

Let us finally consider the total effect of the various cosmological parameters on the C_ℓ spectrum. The C_ℓ provides the most important single observational data set for determining (or constraining) cosmological parameters, since it has a rich structure which we can measure with an accuracy that other cosmological observations cannot match, and because it depends on so many different cosmological parameters in many ways. The latter is both a strength and weakness: the number of cosmological parameters we can determine is large, but on the other hand, some feature in C_ℓ may be caused by more than one parameter, so that we may only be able to constrain some combination of such parameters, not the parameters individually. We say that such parameters are *degenerate* in the CMB data. Other cosmological observations are then needed to break such degeneracies.

We shall consider 7 "standard parameters":

- Ω_0 total density parameter
- Ω_Λ cosmological constant (or vacuum energy) density parameter
- A amplitude of primordial scalar perturbations (at some pivot scale k_p)
- n spectral index of primordial scalar perturbations
- τ optical depth due to reionization (discussed in Sec. 12.9.6)
- $\omega_b \equiv \Omega_b h^2$ "physical" baryon density parameter
- $\omega_m \equiv \Omega_m h^2$ "physical" matter density parameter

There are other possible cosmological parameters ("additional parameters") which might affect the C_ℓ spectrum, e.g.,

- m_{ν_i} neutrino masses
- w dark energy equation-of-state parameter

- $\frac{dn}{d\ln k}$ scale dependence of the spectral index
- r, n_T relative amplitude and spectral index of tensor perturbations
- B, $n_{\rm iso}$ amplitudes and spectral indices of primordial isocurvature perturbations
- $A_{\rm cor}$, $n_{\rm cor}$ and their correlation with primordial curvature perturbations

We assume here that these additional parameters have no impact, i.e., they have the "standard" values

$$m_{\nu_i} = r = \frac{dn}{d\ln k} = B = A_{\rm cor} = 0\,, \quad w = -1 \tag{107}$$

to the accuracy which matters for C_ℓ observations. This is both observationally and theoretically reasonable. There is no sign in the present-day CMB data for deviations from these values. On the other hand, significant deviations can be consistent with the data, and may be discovered by future CMB (and other) observations, in particular the Planck satellite. The primordial isocurvature perturbations refer to the possibility that the primordial scalar perturbations are not adiabatic, and therefore are not completely determined by the comoving curvature perturbation $\mathcal{R}$.

The assumption that these additional parameters have no impact, leads to a determination of the standard parameters with an accuracy that may be too optimistic, since the standard parameters may have degeneracies with the additional parameters.

12.9.1 Independent vs. dependent parameters

The above is our choice of independent cosmological parameters. Ω_m, Ω_b and H_0 (or h) are then dependent (or "derived") parameters, since they are determined by

$$\Omega_0 = \Omega_m + \Omega_\Lambda \quad \Rightarrow \quad \Omega_m = \Omega_0 - \Omega_\Lambda \tag{108}$$

$$h = \sqrt{\frac{\omega_m}{\Omega_m}} = \sqrt{\frac{\omega_m}{\Omega_0 - \Omega_\Lambda}} \tag{109}$$

$$\Omega_b = \frac{\omega_b}{h^2} = \frac{\omega_b}{\omega_m}(\Omega_0 - \Omega_\Lambda) \tag{110}$$

Note in particular, that the Hubble constant H_0 is now a dependent parameter! We cannot vary it independently, but rather the varying of ω_m, Ω_0, or Ω_Λ also causes H_0 to change.

Different choices of independent parameters are possible within our 7-dimensional parameter space (e.g., we could have chosen H_0 to be an independent parameter and let Ω_Λ to be a dependent parameter instead). They can be though of as different coordinate systems[8] in this 7-dim space. *It is not meaningful to discuss the effect of one parameter without specifying which is your set of independent parameters!*

Some choices of independent parameters are better than others. The above choice represents standard practice in cosmology today.[9] The independent parameters have

[8] The situation is analogous to the choice of independent thermodynamic variables in thermodynamics.

[9] There are other choices in use, that are even more geared to minimizing parameter degeneracy. For example, the sound horizon angle ϑ_s may be used instead of Ω_Λ as an independent parameter, since it is directly determined by the acoustic peak separation. However, since the determination of the dependent parameters from it is complicated, such use is more directed towards technical data analysis than pedagogical discussion.

been chosen so that they correspond as directly as possible to physics affecting the C_ℓ spectrum and thus to observable features in it. We want the effects of our independent parameters on the observables to be as different ("orthogonal") as possible in order to avoid parameter degeneracy.

In particular,

- ω_m (not Ω_m) determines $z_{\rm eq}$ and $k_{\rm eq}$, and thus, e.g., the magnitude of the early ISW effect and which scales enter during matter- or radiation-dominated epoch.
- ω_b (not Ω_b) determines the baryon/photon ratio and thus, e.g., the relative heights of the odd and even peaks.
- Ω_Λ (not $\Omega_\Lambda h^2$) determines the late ISW effect.

There are many effects on the C_ℓ spectrum, and parameters act on them in different combinations. Thus there is no perfectly "clean" way of choosing independent parameters. Especially having the Hubble constant as a dependent parameter takes some getting used to.

In the following CAMB[10] plots we see the effect of these parameters on C_ℓ by varying one parameter at a time around a *reference model*, whose parameters have the following values.

Independent parameters:

$$\begin{aligned} \Omega_0 &= 1 & \Omega_\Lambda &= 0.7 \\ A &= 1 & \omega_m &= 0.147 \\ n &= 1 & \omega_b &= 0.022 \\ \tau &= 0.1 \end{aligned}$$

which give for the dependent parameters

$$\begin{aligned} \Omega_m &= 0.3 & h &= 0.7 \\ \Omega_c &= 0.2551 & \omega_c &= 0.125 \\ \Omega_b &= 0.0449 \end{aligned}$$

The meaning of setting $A = 1$ is just that the resulting C_ℓ still need to be multiplied by the true value of A^2. (In this model the true value should be about $A = 5 \times 10^{-5}$ to agree with observations.) If we really had $A = 1$, perturbation theory of course would not be valid! This is a relatively common practice, since the effect of changing A is so trivial, it makes not much sense to plot C_ℓ separately for different values of A.

12.9.2 Sound horizon angle

The positions of the acoustic peaks of the C_ℓ spectrum provides us with a measurement of the sound horizon angle

$$\vartheta_s \equiv \frac{r_s(t_{\rm dec})}{d_A^c(t_{\rm dec})}$$

[10] CAMB is a publicly available code for precise calculation of the C_ℓ spectrum. See http://camb.info/

We can use this in the determination of the values of the cosmological parameters, once we have calculated how this angle depends on those parameters. It is the ratio of two quantities, the sound horizon at photon decoupling, $r_s(t_{\rm dec})$, and the angular diameter distance to the last scattering, $d_A^c(t_{\rm dec})$.

Angular diameter distance to last scattering

The angular diameter distance $d_A^c(t_{\rm dec})$ to the last scattering surface we have already calculated and it is given by Eq. (32) as

$$d_A^c(t_{\rm dec}) = H_0^{-1}\frac{1}{\sqrt{|\Omega_0-1|}}\,S_k\left(\sqrt{|\Omega_0-1|}\int_{\frac{1}{1+z_{\rm dec}}}^{1}\frac{dx}{\sqrt{\Omega_0(x-x^2)-\Omega_\Lambda(x-x^4)+x^2}}\right), \tag{111}$$

from which we see that it depends on the three cosmological parameters H_0, Ω_0 and Ω_Λ. Here $\Omega_0 = \Omega_m + \Omega_\Lambda$, so we could also say that it depends on H_0, Ω_m, and Ω_Λ, but it is easier to discuss the effects of these different parameters if we keep Ω_0 as an independent parameter, instead of Ω_m, since the "geometry effect" of the curvature of space, which determines the relation between the comoving angular diameter distance d_A^c and the comoving distance d^c, is determined by Ω_0.

1. The comoving angular diameter distance is inversely proportional to H_0 (directly proportional to the Hubble distance H_0^{-1}).

2. Increasing Ω_0 decreases $d_A^c(t_{\rm dec})$ in relation to $d^c(t_{\rm dec})$ because of the geometry effect.

3. With a fixed Ω_Λ, increasing Ω_0 decreases $d^c(t_{\rm dec})$, since it means increasing Ω_m, which has a decelerating effect on the expansion. With a fixed present expansion rate H_0, deceleration means that expansion was faster earlier $\Rightarrow$ universe is younger $\Rightarrow$ there is less time for photons to travel as the universe cools from $T_{\rm dec}$ to T_0 $\Rightarrow$ last scattering surface is closer to us.

4. Increasing Ω_Λ (with a fixed Ω_0) increases $d^c(t_{\rm dec})$, since it means a larger part of the energy density is in dark energy, which has an accelerating effect on the expansion. With fixed H_0, this means that expansion was slower in the past $\Rightarrow$ universe is older $\Rightarrow$ more time for photons $\Rightarrow$ last scattering surface is further out. $\therefore$ Ω_Λ increases $d_A^c(t_{\rm dec})$.

Here 2 and 3 work in the same direction: increasing Ω_0 decreases $d_A^c(t_{\rm dec})$, but the geometry effect (2) is stronger. See Fig. 11 for the case $\Omega_\Lambda = 0$, where the dashed line (the comoving distance) shows effect (3) and the solid line (the comoving angular diameter distance) the combined effect (2) and (3).

However, now we have to take into account that, in our chosen parametrization, H_0 is not an independent parameter, but

$$H_0^{-1} \propto \sqrt{\frac{\Omega_0-\Omega_\Lambda}{\omega_m}},$$

so that via H_0^{-1}, Ω_0 increases and Ω_Λ decreases $d_A^c(t_{\rm dec})$, which are the opposite effects to those discussed above. For Ω_Λ this opposite effect wins. See Figs. 19 and 20.

Sound horizon

To calculate the sound horizon,

$$r_s(t_{\rm dec}) = a_0 \int_0^{t_{\rm dec}} \frac{c_s(t)}{a(t)} dt = \int_0^{t_{\rm dec}} \frac{dt}{x} c_s(t) = \int_0^{x_{\rm dec}} \frac{dx}{x \cdot (dx/dt)} c_s(x)\,, \qquad (112)$$

we need the speed of sound, from Eq. (79),

$$c_s^2(x) = \frac{1}{3} \frac{1}{1 + \frac{3}{4}\frac{\bar{\rho}_b}{\bar{\rho}_\gamma}} = \frac{1}{3} \frac{1}{1 + \frac{3}{4}\frac{\omega_b}{\omega_\gamma} x}\,, \qquad (113)$$

where $x \equiv a/a_0$ (as in Eq. (111) also), and the upper limit of the integral is $x_{\rm dec} = 1/(1 + z_{\rm dec})$.

The other element in the integrand of Eq. (112) is the expansion law $a(t)$ before decoupling. From Chapter 4 we have that

$$x\frac{dx}{dt} = H_0 \sqrt{\Omega_\Lambda x^4 + (1 - \Omega_0) x^2 + \Omega_m x + \Omega_r}\,. \qquad (114)$$

In the integral (111) we dropped the Ω_r, since it is important only at early times, and the integral from $x_{\rm dec}$ to 1 is dominated by late times. Integral (112), on the other hand, includes only early times, and now we can instead drop the Ω_Λ and $1 - \Omega_0$ terms (i.e., we can ignore the effect of curvature and dark energy in the early universe, before photon decoupling), so that

$$x\frac{dx}{dt} \approx H_0 \sqrt{\Omega_m x + \Omega_r} = H_{100} \sqrt{\omega_m x + \omega_r} = \frac{\sqrt{\omega_m x + \omega_r}}{2998 \text{ Mpc}}\,, \qquad (115)$$

where we have written

$$H_0 \equiv h \cdot 100 \frac{\text{km/s}}{\text{Mpc}} \equiv h \cdot H_{100} = \frac{h}{2997.92 \text{ Mpc}}\,. \qquad (116)$$

Thus the sound horizon is given by

$$\begin{aligned} r_s(x) &= 2998 \text{ Mpc} \int_0^x \frac{c_s(x) dx}{\sqrt{\omega_m x + \omega_r}} \\ &= 2998 \text{ Mpc} \cdot \frac{1}{\sqrt{3\omega_r}} \int_0^x \frac{dx}{\sqrt{\left(1 + \frac{\omega_m}{\omega_r} x\right)\left(1 + \frac{3}{4}\frac{\omega_b}{\omega_\gamma} x\right)}}\,. \end{aligned} \qquad (117)$$

Here

$$\omega_\gamma = 2.4702 \times 10^{-5} \qquad \text{and} \qquad (118)$$

$$\omega_r = \left[1 + \frac{7}{8} N_\nu \left(\frac{4}{11}\right)^{4/3}\right] \omega_\gamma = 1.6904\, \omega_\gamma = 4.1756 \times 10^{-5} \qquad (119)$$

are accurately known from the CMB temperature $T_0 = 2.725$ K (and therefore we do not consider them as cosmological parameters in the sense of something to be determined from the C_ℓ spectrum).

Thus the sound horizon depends on the two cosmological parameters ω_m and ω_b,

$$r_s(t_{\rm dec}) = r_s(\omega_m, \omega_b)$$

From Eq. (117) we see that increasing either ω_m or ω_b *makes the sound horizon at decoupling,* $r_s(x_{\rm dec})$*, shorter*:

- ω_b slows the sound down
- ω_m speeds up the expansion at a given temperature, so the universe cools to $T_{\rm dec}$ in less time.

The integral (117) can be done and it gives

$$r_s(t_{\rm dec}) = \frac{2998\ {\rm Mpc}}{\sqrt{1+z_{\rm dec}}} \frac{2}{\sqrt{3\omega_m R_*}} \ln \frac{\sqrt{1+R_*}+\sqrt{R_*+r_*R_*}}{1+\sqrt{r_*R_*}}\,, \tag{120}$$

where

$$r_* \equiv \frac{\bar\rho_r(t_{\rm dec})}{\bar\rho_m(t_{\rm dec})} = \frac{\omega_r}{\omega_m}\frac{1}{x_{\rm dec}} = 0.0459\frac{1}{\omega_m}\left(\frac{1+z_{\rm dec}}{1100}\right) \tag{121}$$

$$R_* \equiv \frac{3\bar\rho_b(t_{\rm dec})}{4\bar\rho_\gamma(t_{\rm dec})} = \frac{3\omega_b}{4\omega_\gamma}x_{\rm dec} = 27.6\,\omega_b\left(\frac{1100}{1+z_{\rm dec}}\right)\,. \tag{122}$$

For our reference values $\omega_m = 0.147$, $\omega_b = 0.022$, and $1+z_{\rm dec} = 1100$[11] we get $r_* = 0.312$ and $R_* = 0.607$ and $r_s(t_{\rm dec}) = 143$ Mpc for the sound horizon at decoupling.

Summary

The angular diameter distance $d_A^c(t_{\rm dec})$ is the most naturally discussed in terms of H_0, Ω_0, and Ω_Λ, but since these are not the most convenient choice of independent parameters for other purposes, we shall trade H_0 for ω_m according to Eq. (109). Thus we have that the sound horizon angle depends on 4 parameters,

$$\vartheta_s \equiv \frac{r_s(\omega_m,\omega_b)}{d_A^c(\Omega_0,\Omega_\Lambda,\omega_m)} = \vartheta_s(\Omega_0,\Omega_\Lambda,\omega_m,\omega_b) \tag{123}$$

12.9.3 Acoustic peak heights

There are a number of effects affecting the heights of the acoustic peaks:

1. **The early ISW effect.** The early ISW effect raises the first peak. It is caused by the evolution of Φ because of the effect of the radiation contribution on the expansion law after $t_{\rm dec}$. This depends on the radiation-matter ratio at that time; decreasing ω_m makes the early ISW effect stronger.

2. **Shift of oscillation equilibrium by baryons.** (Baryon drag.) This makes the odd peaks (which correspond to compression of the baryon-photon fluid in the potential wells, decompression on potential hills) higher, and the even peaks (decompression at potential wells, compression on top of potential hills) lower.

3. **Baryon damping.** The time evolution of $R \equiv 3\bar\rho_b/4\bar\rho_\gamma$ causes the amplitude of the acoustic oscillations to be damped in time roughly as $(1+R)^{-1/4}$. This reduces the amplitudes of all peaks.

[11] Photon decoupling temperature, and thus $1+z_{\rm dec}$, depends somewhat on ω_b, but since this dependence is not easy to calculate (recombination and photon decoupling were discussed in Chapter 6), we have mostly ignored this dependence and used the fixed value $1+z_{\rm dec} = 1100$.

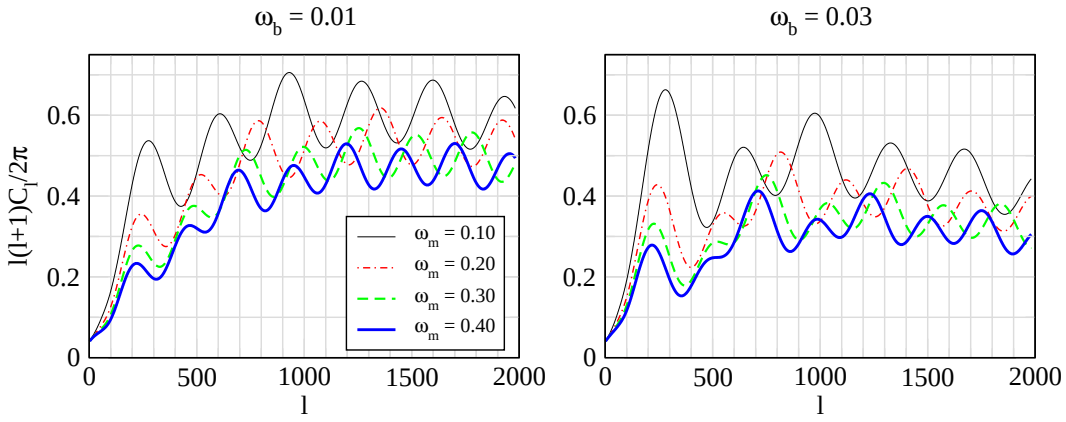

Figure 17: The effect of ω_m. The angular power spectrum C_ℓ is here calculated without the effect of diffusion damping, so that the other effects on peak heights could be seen more clearly. Notice how reducing ω_m raises all peaks, but the effect on the first few peaks is stronger in relative terms, as the radiation driving effect is extended towards larger scales (smaller ℓ). The first peak is raised mainly because the ISW effect becomes stronger. Figure and calculation by R. Keskitalo.

4. **Radiation driving.**[12] This is an effect related to horizon scale physics that we have not tried to properly calculate. For scales k which enter during the radiation-dominated epoch, or near matter-radiation equality, the potential Φ decays around the time when the scale enters. The potential keeps changing as long as the radiation contribution is important, but the largest change in Φ is around horizon entry. Because the sound horizon and Hubble length are comparable, horizon entry and the corresponding potential decay always happen during the first oscillation period. This means that the baryon-photon fluid is falling into a deep potential well, and therefore is compressed by gravity by a large factor, before the resulting overpressure is able to push it out. Meanwhile the potential has decayed, so it is less able to resist the decompression phase, and the overpressure is able to kick the fluid further out of the well. This increases the amplitude of the acoustic oscillations. The effect is stronger for the smaller scales which enter when the universe is more radiation-dominated, and therefore raises the peaks with a larger peak number m more. Reducing ω_m makes the universe more radiation dominated, making this effect stronger and extending it towards the peaks with lower peak number m.

5. **Diffusion damping.** Diffusion damping lowers the heights of the peaks. It acts in the opposite direction than the radiation driving effect, lowering the peaks with a larger peak number m more. Because the diffusion damping effect is exponential in ℓ, it wins for large ℓ.

Effects 1 and 4 depend on ω_m, effects 2, 3, and 5 on ω_b.

See Figs. 17 and 18 for the effects of ω_m and ω_b on peak heights.

[12] This is also called gravitational driving, which is perhaps more appropriate, since the effect is due to the change in the gravitational potential.

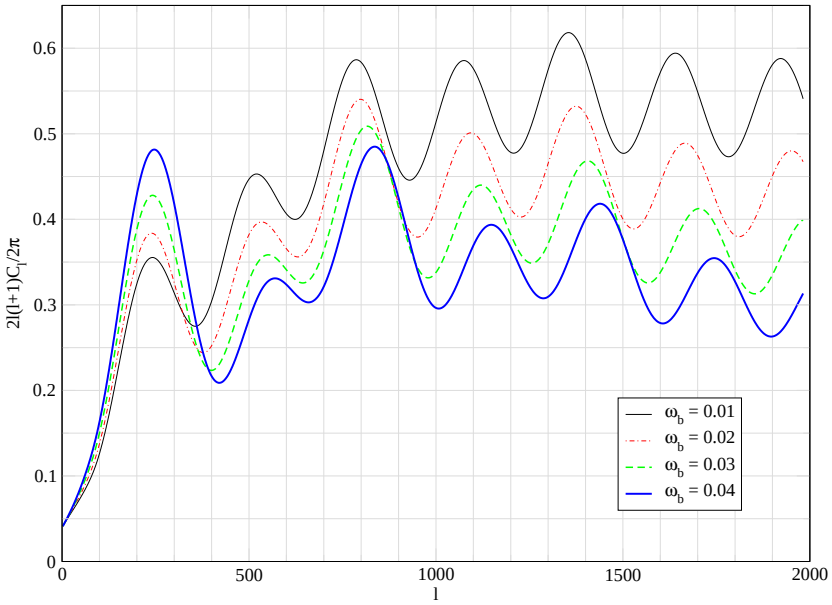

Figure 18: The effect of ω_b. The angular power spectrum C_ℓ is here calculated without the effect of diffusion damping, so that the other effects on peak heights could be seen more clearly. Notice how increasing ω_b raises odd peaks relative to the even peaks. Because of baryon damping there is a general trend downwards with increasing ω_b. This figure is for $\omega_m = 0.20$. Figure and calculation by R. Keskitalo.

12.9.4 Effect of Ω_0 and Ω_Λ

These two parameters have only two effects:

1. they affect the sound horizon angle and thus the positions of the acoustic peaks
2. they affect the late ISW effect

See Figs. 19 and 20. Since the late ISW effect is in the region of the C_ℓ spectrum where the cosmic variance is large, it is difficult to detect. Thus we can in practice only use ϑ_s to determine Ω_0 and Ω_Λ. Since ω_b and ω_m can be determined quite accurately from C_ℓ acoustic peak heights, peak separation, i.e., ϑ_s, can then indeed be used for the determination of Ω_0 and Ω_Λ. Since one number cannot be used to determine two, the parameters Ω_0 and Ω_Λ are degenerate. CMB observations alone cannot be used to determine them both. Other cosmological observations (like the power spectrum $P_\delta(k)$ from large scale structure, or the SNIa redshift-distance relationship) are needed to break this degeneracy.

A fixed ϑ_s together with fixed ω_b and ω_m determine a line on the (Ω_0, Ω_Λ) - plane. See Fig. 21. Derived parameters, e.g., h, vary along that line. As you can see from Figs. 19 and 20, changing Ω_0 (around the reference model) affects ϑ_s much more strongly than changing Ω_Λ. This means that the orientation of the line is such that Ω_Λ varies more rapidly along that line than Ω_0. Therefore using additional constraints from other cosmological observations, e.g. the Hubble Space Telescope determination of h based on the distance ladder, which select a short section from that line, gives us a fairly good determination of Ω_0, leaving the allowed range for Ω_Λ still quite large.

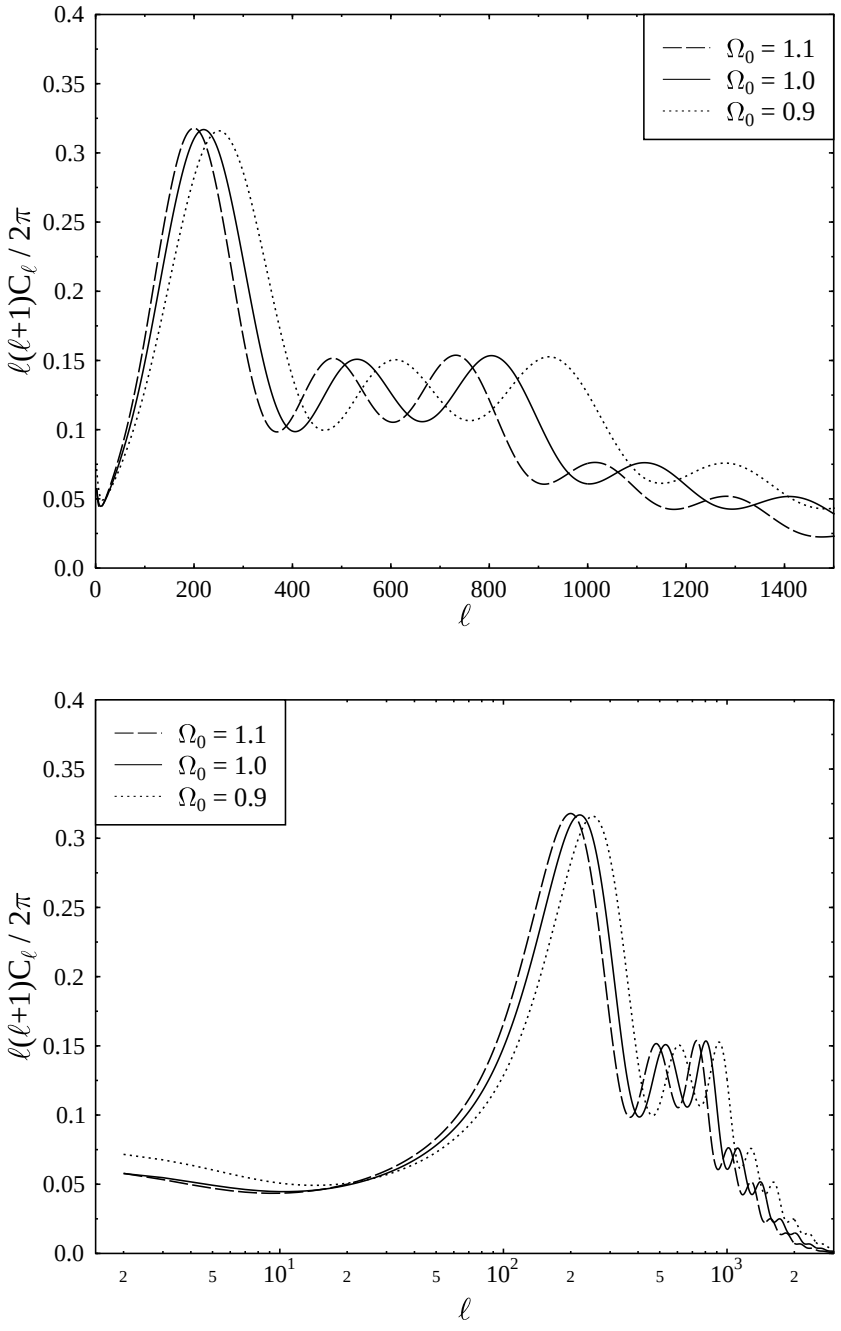

Figure 19: The effect of changing Ω_0 from its reference value $\Omega_0 = 1$. The top panel shows the C_ℓ spectrum with a linear ℓ scale so that details at larger ℓ where cosmic variance effects are smaller can be better seen. The bottom plot has a logarithmic ℓ scale so that the integrated Sachs-Wolfe effect at small ℓ can be better seen. The logarithmic scale also makes clear that the effect of the change in sound horizon angle is to stretch the spectrum by a constant factor in ℓ space.

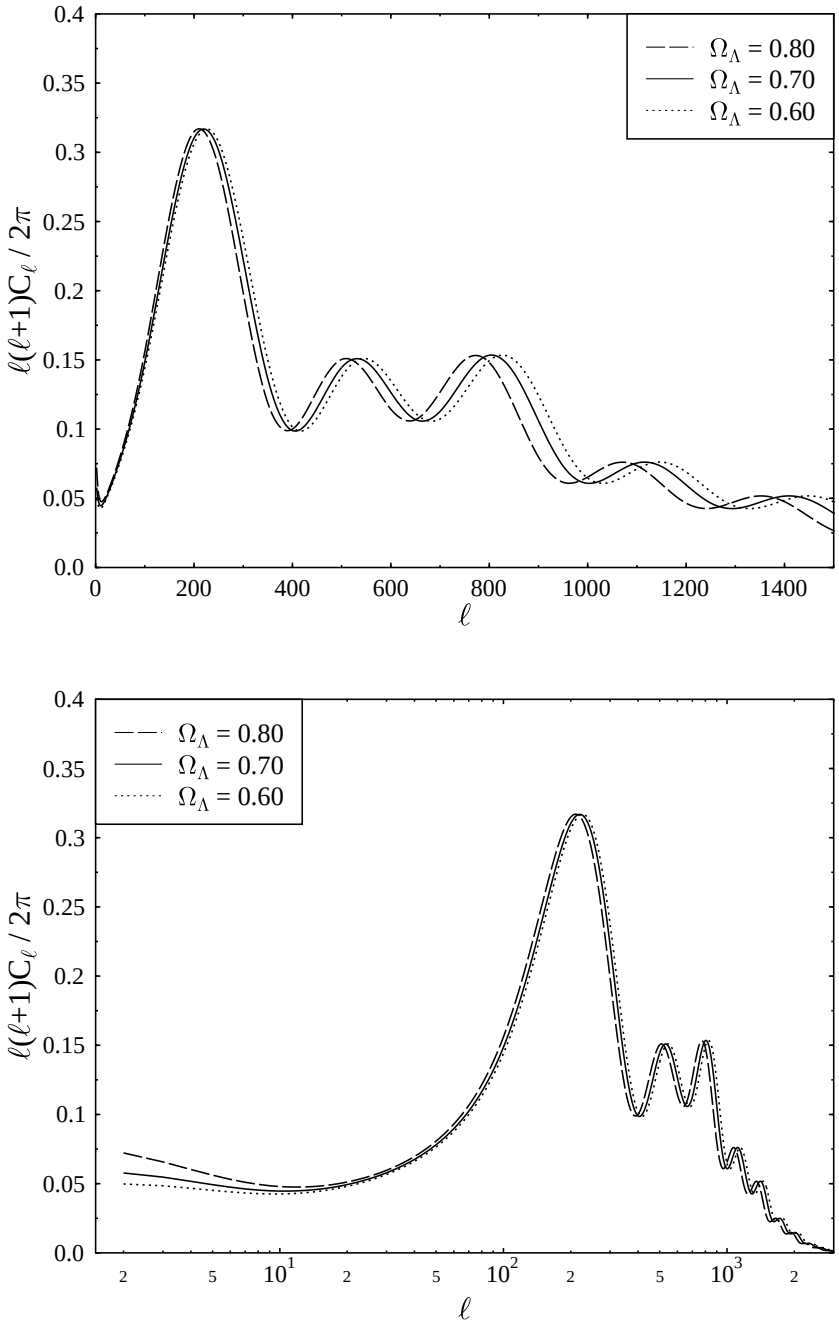

Figure 20: The effect of changing Ω_Λ from its reference value $\Omega_\Lambda = 0.7$.

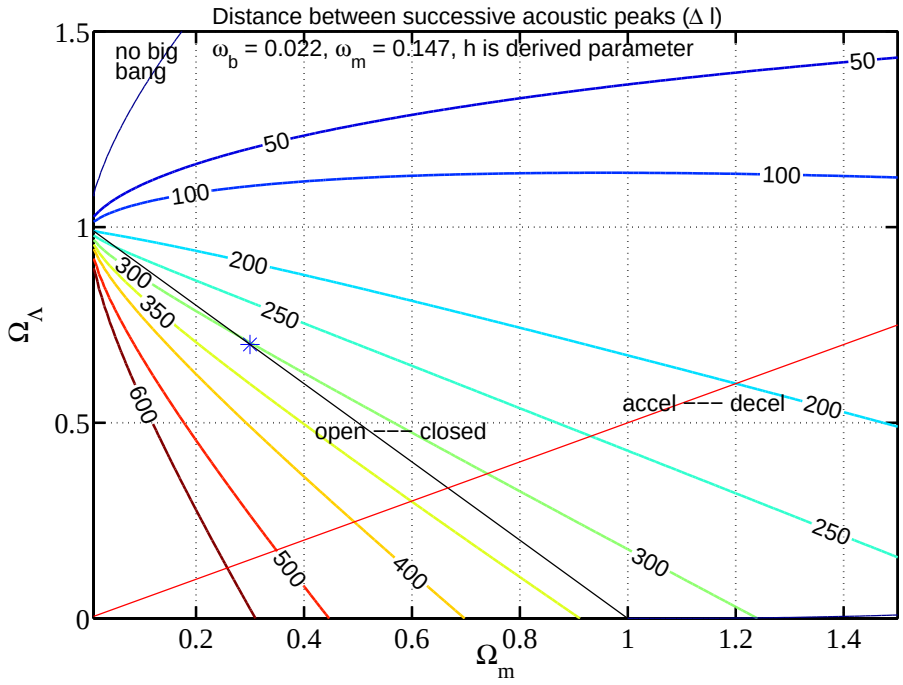

Figure 21: The lines of constant sound horizon angle ϑ_s on the $(\Omega_m,\Omega_\Lambda)$ plane for fixed ω_b and ω_m. The numbers on the lines refer to the corresponding acoustic scale $\ell_A \equiv \pi/\vartheta_s$ ($\sim$ peak separation) in multipole space. Figure by J. Väliviita. See his PhD thesis[9], p.70, for an improved version including the HST constraint on h.

Therefore it is often said that CMB measurements have determined that $\Omega_0 \sim 1$. But as explained above, this determination necessary requires the use of some auxiliary cosmological data besides the CMB.

12.9.5 Effect of the primordial spectrum

The effect of the primordial spectrum is simple: raising the amplitude A raises the C_ℓ also, and tilting the primordial spectrum tilts the C_ℓ also. See Figs. 22 and 23.

12.9.6 Optical depth due to reionization

When radiation from the first stars reionizes the intergalactic gas, CMB photons may scatter from the resulting free electrons. The optical depth τ due to reionization is the expectation number of such scatterings per CMB photon. It is expected to be about 0.1 or less, i.e., most CMB photons do not scatter at all. This rescattering causes additional polarization of the CMB, and CMB polarization measurements are actually the best way to determine τ.

The WMAP first year results (the observed temperature-polarization correlation spectrum $\widehat{C}_\ell^{TE}$) seemed to indicate a value greater than 0.1. This would have meant that reionization occurred earlier (at a higher redshift) than had been thought, meaning that the first stars formed rather early, when the universe was just a few hundred million years old. However, this scare went away, as the third year WMAP results give $\tau < 0.1$.

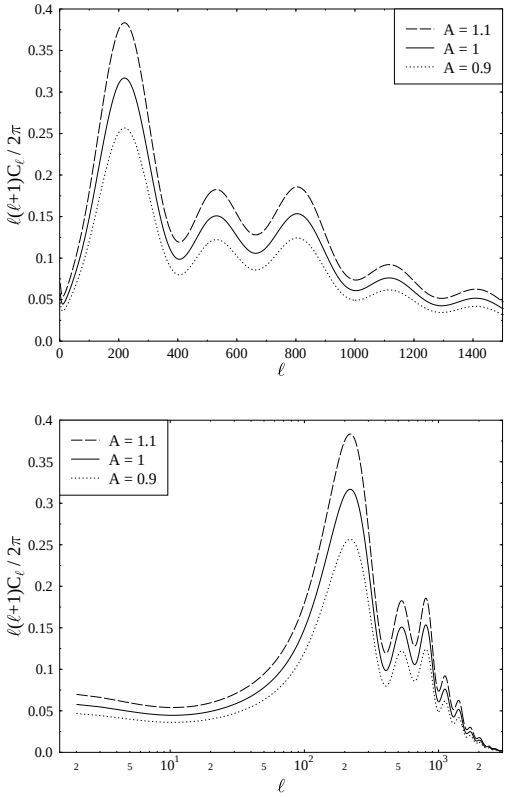

Figure 22: The effect of changing the primordial amplitude from its reference value $A = 1$.

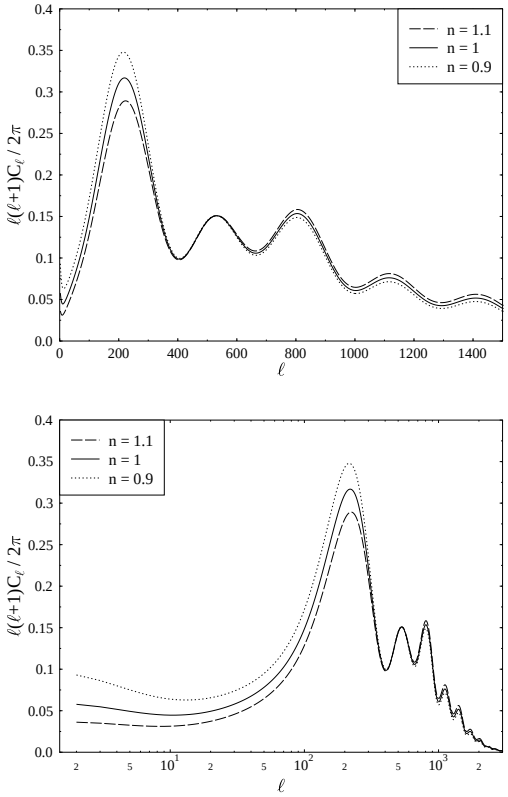

Figure 23: The effect of changing the spectral index from its reference value $n = 1$.

Because of this scattering, not all the CMB photons come from the location on the last scattering surface we think they come from. The effect of the rescattered photons is to mix up signals from different directions and therefore to reduce the CMB anisotropy. The reduction factor on $\delta T/T$ is $e^{-\tau}$ and on the C_ℓ spectrum $e^{-2\tau}$. However, this does not affect the largest scales, scales larger than the area from which the rescattered photons reaching us from a certain direction, originally came from. Such a large-scale anisotropy has affected all such photons the same way, and thus is not lost in the mixing. See Fig. 24.

12.9.7 Effect of ω_b and ω_m

These parameters affect both the positions of the acoustic peaks (through ϑ_s) and the heights of the different peaks. The latter effect is the more important, since both parameters have their own signature on the peak heights, allowing an accurate determination of these parameters, whereas the effect on ϑ_s is degenerate with Ω_0 and Ω_Λ.

Especially ω_b has a characteristic effect on peak heights: Increasing ω_b raises the odd peaks and reduces the even peaks, because it shifts the balance of the acoustic oscillations (the $-R\Phi$ effect). This shows the most clearly at the first and second peaks.[13] Raising ω_b also shortens the damping scale k_D^{-1} due to photon diffusion, moving the corresponding damping scale ℓ_D of the C_ℓ spectrum towards larger ℓ. This has the effect of raising C_ℓ at large ℓ. See Fig. 25.

Increasing ω_m makes the universe more matter dominated at $t_{\rm dec}$ and therefore it reduces the early ISW effect, making the first peak lower. This also affects the shape of the first peak.

The "radiation driving" effect is most clear at the second to fourth peaks. Reducing ω_m makes these peaks higher by making the universe more radiation-dominated at the time the scales corresponding to these peaks enter, and thus strengthening this radiation driving. The fifth and further peaks correspond to scales that have anyway essentially the full effect, whereas for the first peak this effect is anyway weak. (We see instead the ISW effect in the first peak.) See Fig. 26.

12.10 Best Values for the Cosmological Parameters

The most important cosmological data set for determining the values for the cosmological parameters is the WMAP data [3, 4] on the CMB anisotropy, because of its accurate measurement of the first and second peaks of the C_ℓ spectrum. Since the resolution of the WMAP is not good enough for an accurate measurement of the third peak and does not cover higher ℓ it can be supplemented with CMB measurements from ground-based and balloon-borne instruments with higher resolution but poorer sensitivity and sky coverage. The most accurate measurements for the higher multipoles to date (2008) are from the Arcminute Cosmology Bolometer Array Receiver (ACBAR) [7]. Other relevant high-resolution CMB data sets are those from the balloon-borne Boomerang instrument, the Cosmic Background Imager (CBI), and the Very Small Array (VSA).

[13] There is also an overall "baryon damping effect" on the acoustic oscillations which we have not calculated. It is due to the time dependence of $R \equiv 3\bar{\rho}_b/4\bar{\rho}_m$, which reduces the amplitude of the oscillation by about $(1+R)^{-1/4}$. This explains why the third peak in Fig. 25 is no higher for $\omega_b = 0.030$ than it is for $\omega_b = 0.022$.

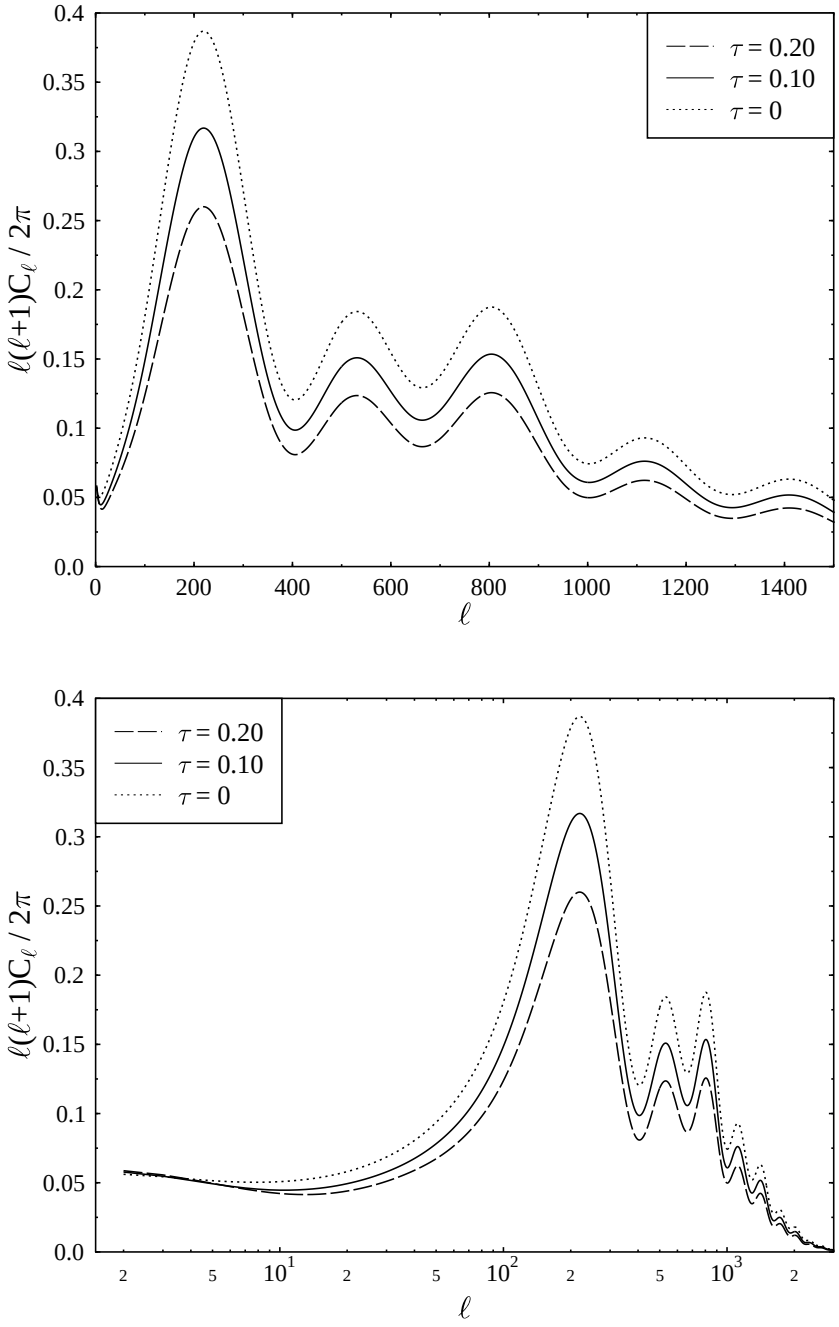

Figure 24: The effect of changing the optical depth from its reference value $\tau = 0.1$.

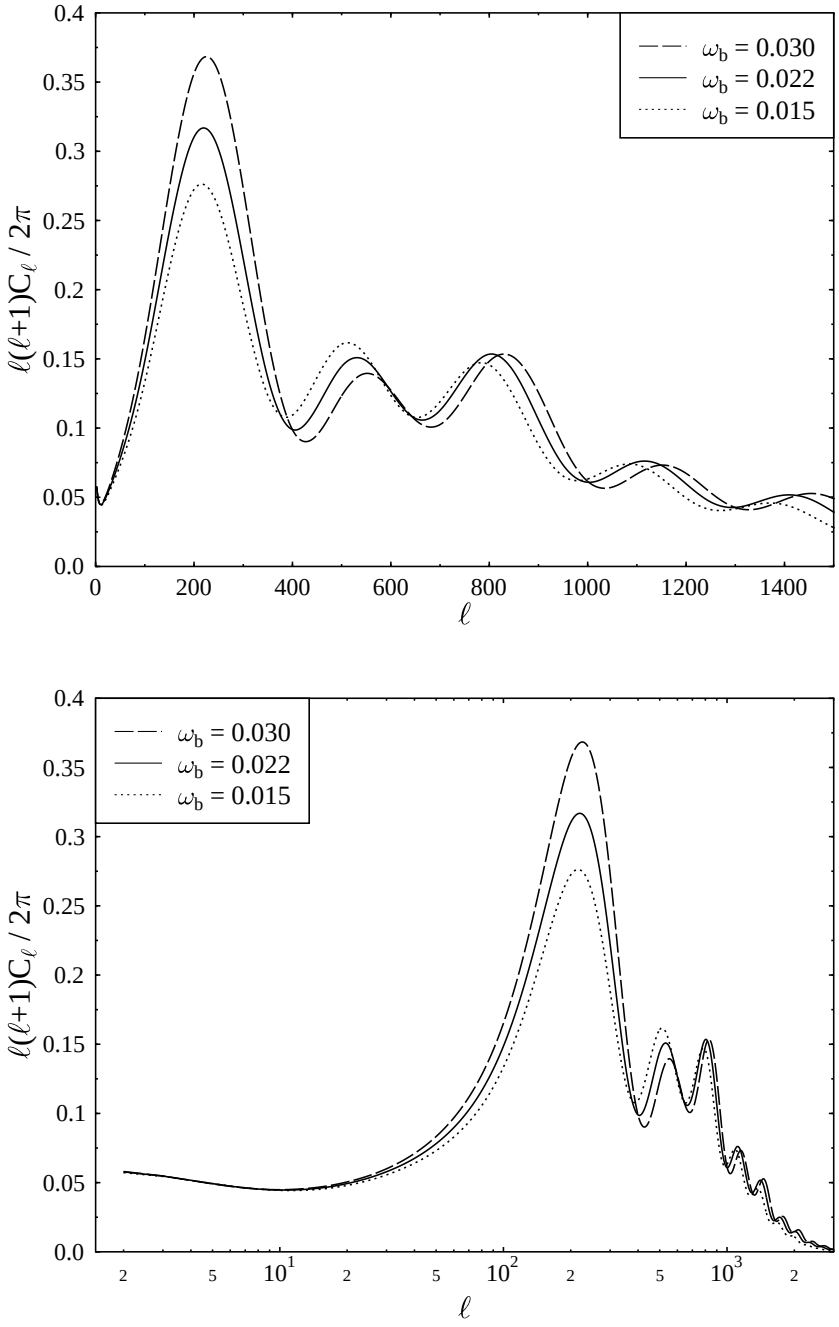

Figure 25: The effect of changing the physical baryon density parameter from its reference value $\omega_b = 0.022$.

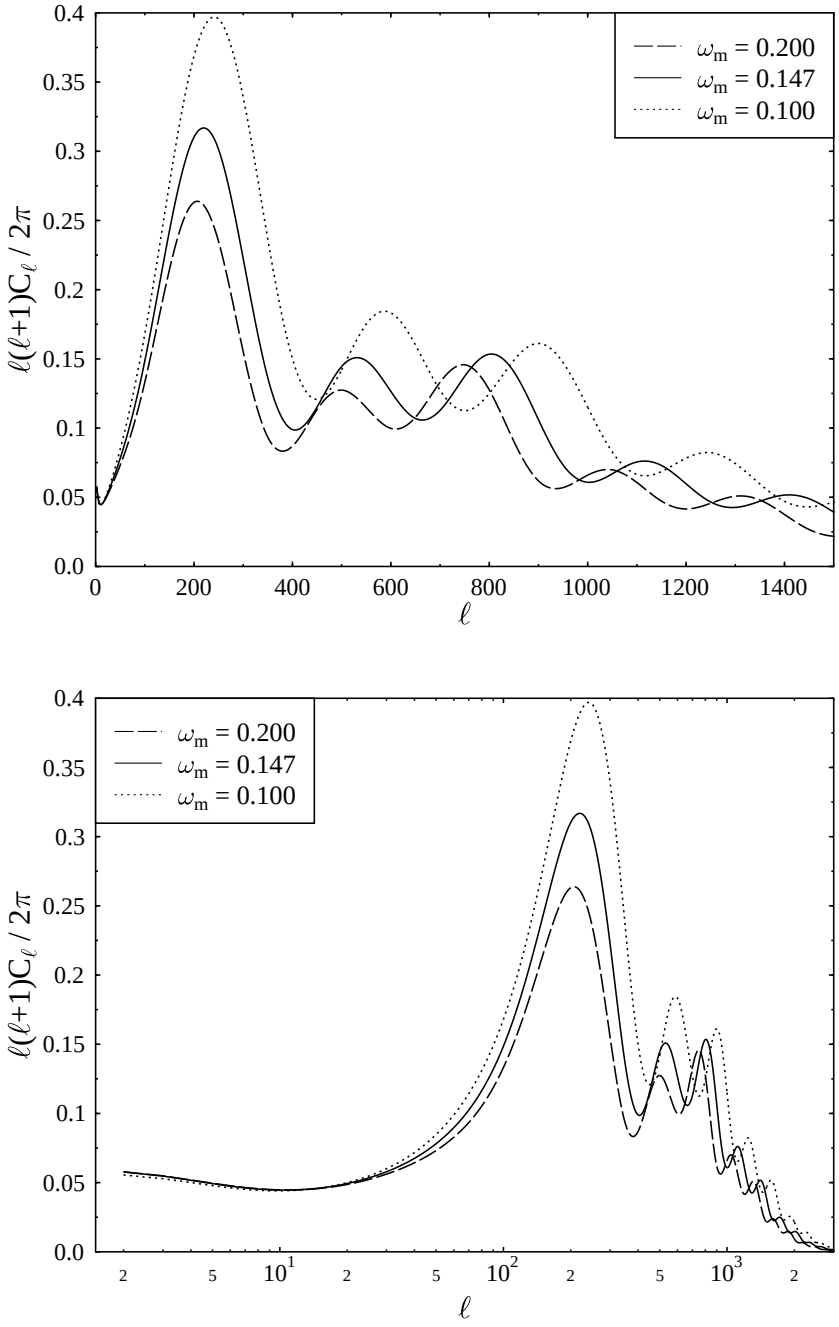

Figure 26: The effect of changing the physical matter density parameter from its reference value $\omega_m = 0.147$.

Because of degeneracies of cosmological parameters in the CMB data, most importantly the Ω_0-Ω_Λ degeneracy, CMB observations have to be supplemented by other cosmological data for a good determination of the main cosmological parameters.

Large scale structure surveys, i.e., the measurement of the 3-dimensional matter power spectrum $P_\delta(k)$ from the distribution of galaxies, mainly measure the combination $\Omega_m h$, since this determines where $P_\delta(k)$ turns down. Actually it turns down at $k_{\rm eq}$ which is proportional to $\omega_m \equiv \Omega_m h^2$, but since in these surveys the distances to the galaxies are deduced from their redshifts (therefore these surveys are also called galaxy redshift surveys), which give the distances only up to the Hubble constant H_0, these surveys determine $h^{-1}k_{\rm eq}$ instead of $k_{\rm eq}$. This cancels one power of h. Having $\Omega_m h^2$ from CMB and $\Omega_m h$ from the galaxy surveys, gives us both h and $\Omega_m = \Omega_0 - \Omega_\Lambda$, which breaks the Ω_0-Ω_Λ degeneracy.

These measurements of $P_\delta(k)$ are now so accurate that the small residual effect from the acoustic oscillations before photon decoupling can be seen as a weak wavy pattern [11]. This is the same structure which we see in the C_ℓ but now much fainter, since now the baryons have fallen into the CDM potential wells, and the CDM was only mildly affected by these oscillations in the baryon-photon fluid. The half-wavelength of this pattern, however, corresponds to the same sound horizon distance $r_s(t_{\rm dec})$ in both cases.[14] However, now the angular scale on the sky is related to it by the angular diameter distance $d_A^c(z)$ to the much smaller redshifts z of the galaxy survey. This $d_A^c(z)$ has then a different relation to Ω_0, Ω_Λ, and ω_m. Thus, comparing the CMB data to the galaxy surveys gives us the ratio $d_A^c(z)/d_A^c(t_{\rm dec})$, which gives us independent information on these parameters.

The most important large scale structure surveys are the 2-degree Galaxy Redshift Survey (2dFGRS) and the Sloan Digital Sky Survey (SDSS).

Another way to break the Ω_0-Ω_Λ degeneracy, is to use the redshift-distance relationship from Supernova Type Ia surveys.

A number of articles have appeared using different combinations of these data sets to determine cosmological parameters. Some time after the first-year WMAP results (WMAP1) [1] came out, Roos [8] combined the results from five different such determinations to arrive at a "recommended" set of values for the cosmological parameters: See Table I for the 7 "standard parameters", Table II for related "derived parameters", and Table III for some "additional parameters".

The upper and lower limits are "17- and 83-percentiles" which means that there is some relation to having a formal 66% probability that the correct value is in this range (although Roos explicitly says that no "probability measure" should be associated with his method).

After this compilation, both WMAP and SDSS have come up with new, more accurate results. The WMAP 3-year data (WMAP3) [2] was published in 2006 and the 5-year data (WMAP5) [3, 4] in 2008. We show the parameter determinations both from WMAP3 only (WMAP3) and WMAP3 combined with SDSS luminous red galaxy data (WMAP3+SDSS LRG) [10] in Tables I-III. (The primordial amplitude A is not given for WMAP3 and SDSS in Table I, since they had used a differently defined parameter to represent this degree of freedom.) Finally, we give

[14] To be accurate, the best $t_{\rm dec}$ value to represent the effect in $P_\delta(k)$, is not exactly the same as for C_ℓ, since photon decoupling was not instantaneous, and in one we are looking at the effect on matter and in the other on photons.

Table I: Standard parameters

	Roos [8]	WMAP3 only	WMAP3 + SDSS LRG	WMAP5 + SNIa + BAO
Ω_0	$1.023^{+0.050}_{-0.017}$		$1.003^{+0.010}_{-0.009}$	1.0045 ± 0.0130
Ω_Λ	$0.727^{+0.031}_{-0.032}$	$0.762^{+0.045}_{-0.027}$	$0.761^{+0.017}_{-0.018}$	0.721 ± 0.015
A	$4.76^{+0.34}_{-0.28} \times 10^{-5}$			$4.94 \pm 0.10 \times 10^{-5}$
n	$0.962^{+0.030}_{-0.027}$	$0.951^{+0.015}_{-0.019}$	0.953 ± 0.016	$0.960^{+0.014}_{-0.013}$
τ	$0.147^{+0.068}_{-0.064}$	0.09 ± 0.03	$0.087^{+0.028}_{-0.030}$	0.084 ± 0.016
ω_b	$0.0227^{+0.0012}_{-0.0013}$	$0.0223^{+0.0007}_{-0.0009}$	$0.0222^{+0.0007}_{-0.0007}$	$0.02265^{+0.00059}_{-0.00059}$
ω_m	0.126 ± 0.016	$0.127^{+0.007}_{-0.013}$	$0.1272^{+0.0044}_{-0.0043}$	0.1369 ± 0.0037

the parameter determinations obtained combining WMAP5 with the acoustic oscillation scale seen in 2dFGRS and SDSS galaxy redshift surveys and with Supernova Type Ia results(WMAP5+BAO+SN) [4]. In [4] the WMAP team decided to use only the baryon acoustic oscillation (BAO) scale part of the 2dFGRS and SDSS results, citing "limited understanding of the consequences of non-linearities" for the shape of the observed $P_\delta(k)$. These non-linearities do not affect the acoustic oscillation scale.

We do not give Ω_0 in the WMAP3 only -column, since this parameter cannot be determined well from CMB data alone, because of the "geometric" degeneracy discussed in Sec. 12.9.4. In fact, WMAP3 data is consistent with a closed universe without dark energy, with $\Omega_0 = \Omega_m \sim 1.3$, and $h \sim 0.3$. Other cosmological data (e.g., the SDSS data on $P_\delta(k)$ is needed to break this degeneracy, and to determine that the universe is flat ($\Omega_0 = 1$) to 1% accuracy. This is illustrated in Figs. 27 and 28. However the remarkable accuracy of this determination, $\Omega_0 = 1.003^{+0.010}_{-0.009}$ comes from the accuracy of the WMAP3 data.

The other parameter estimates in Tables I, II, and III, have been derived under the assumption of a flat universe, $\Omega_0 = 1$, which reduces the uncertainties in them. (This explains why we have an Ω_Λ result in the WMAP3 column).

The median value for the primordial amplitude is

$$A = 4.94 \times 10^{-5}\,. \tag{124}$$

(This WMAP5 result is for a pivot scale $k_p = 0.002$ Mpc^{-1}.) The data favors a slightly red, $n < 1$, spectrum. With WMAP3 this observed deviation from scale-invariance begins to be significant, and can be counted as a major discovery of a new feature in the universe (contrasted to a mere more accurate determination of a parameter).

The uncertainty in τ has decreased with WMAP3 data. This is mainly due to the WMAP measurement of CMB polarization. This is also the main cause for the increased accuracy in the determination of the other parameters by WMAP3, since in the temperature C_ℓ spectrum many parameters are somewhat degenerate with τ.

The BBN limits for ω_b or the Hubble Space Telescope result for h have not been used in obtaining these results, but we see that they are consistent with them.

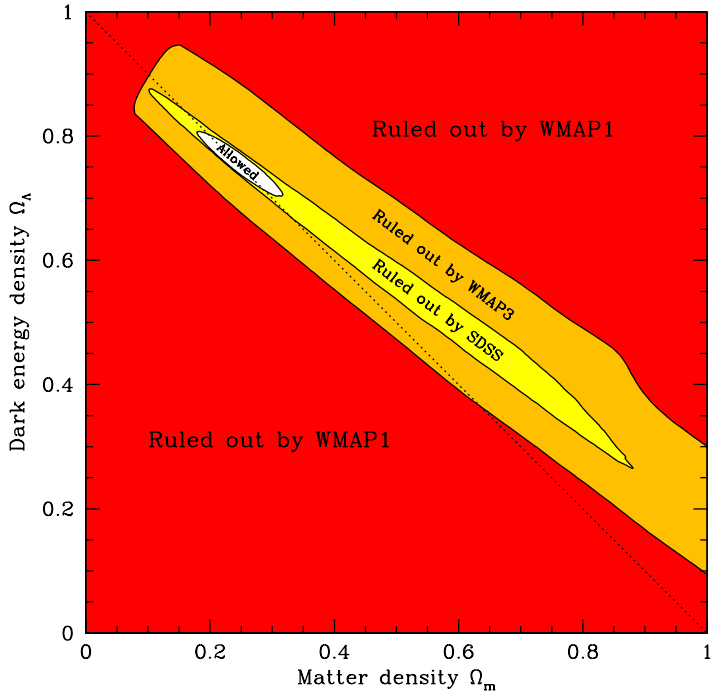

Figure 27: The SDSS data breaks the geometric degeneracy in the WMAP3 data and allows the simultaneous determination of $\Omega_0 \equiv \Omega_m + \Omega_\Lambda$ and Ω_Λ. The WMAP3 constraint shown here actually includes an artificially imposed lower limit for the Hubble constant, $h \geq 0.4$. Without it, the yellow region would extend off the figure. Figure from Tegmark et al. [10]

Table II: Derived parameters

	Roos [8]	WMAP3 only	WMAP3 + SDSS LRG	WMAP5 + SNIa + BAO
Ω_m	$0.273^{+0.031}_{-0.032}$	$0.238^{+0.027}_{-0.045}$	$0.239^{+0.018}_{-0.017}$	0.279 ± 0.015
Ω_c	$0.225^{+0.031}_{-0.032}$		$0.197^{+0.016}_{-0.015}$	0.233 ± 0.013
Ω_b	$0.048^{+0.005}_{-0.004}$		$0.0416^{+0.0019}_{-0.0018}$	$0.0462^{+0.0015}_{-0.0015}$
h	$0.687^{+0.034}_{-0.047}$	$0.73^{+0.03}_{-0.03}$	$0.730^{+0.019}_{-0.019}$	0.701 ± 0.013

Table III: Additional parameters

	Roos [8]	WMAP3 only	WMAP3 + SDSS LRG	WMAP5 + SNIa + BAO
$\sum m_\nu$	< 1.1 eV	< 2.0 eV	< 0.94 eV	< 0.61 eV
w	$-0.93^{+0.13}_{-0.10}$		$-0.941^{+0.087}_{-0.101}$	-0.985 ± 0.063
$\frac{dn}{d\ln k}$	-0.011 ± 0.012	$-0.055^{+0.029}_{-0.035}$	$-0.040^{+0.027}_{-0.027}$	-0.032 ± 0.021
r	< 0.4	< 0.55	< 0.30	< 0.20

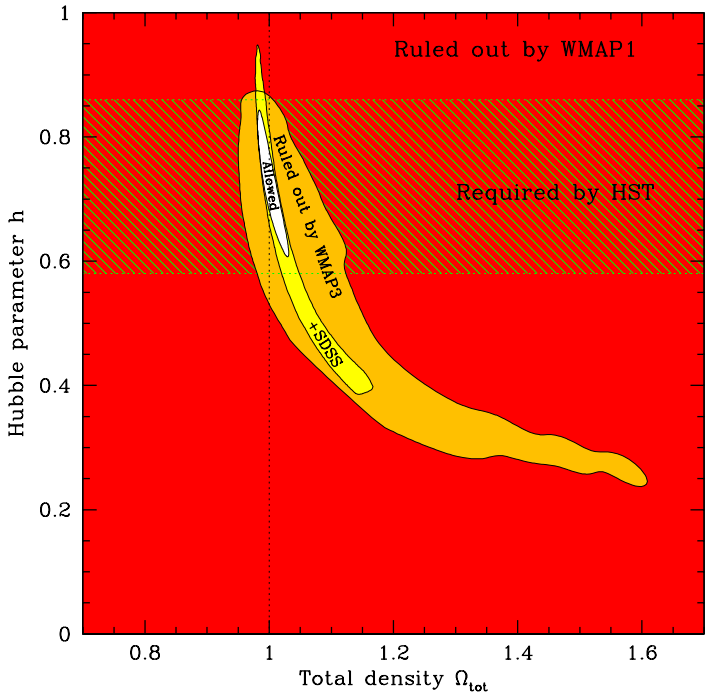

Figure 28: The situation in Fig. 27 illustrated in the (Ω_0, h)-plane. Figure from Tegmark et al. [10]

In Table III the upper limits given for the sum of neutrino masses $\sum m_\nu$ and the ratio $r \equiv A_T^2/A^2$ of tensor perturbations to scalar perturbations are 95% confidence limits. We see that there is no indication in the data for a deviation of these additional parameters from their standard values, except $\frac{dn}{d\ln k}$, for which the data favors a negative value. These standard values (Eq. 107) have been assumed in deriving the results in Tables I and II.

There is no result for the dark energy equation-of-state parameter w in the WMAP3 only -column, since there is a similar geometric degeneracy between w and Ω_Λ (they both show up mainly in the sound horizon angle ϑ_s, and the other effect they have, a late ISW effect, gets lost in cosmic variance) as there is between Ω_0 and Ω_Λ. This is illustrated in Fig. 29.

The value $\frac{dn}{d\ln k} = -0.032$ for a running spectral index would be problematic for inflation, since typical inflation models favor a value much closer to zero. However, the estimated error, ± 0.021, is still large enough so that the result is not significant.

In conclusion, we can say that all cosmological data appear to be consistent with a "vanilla" universe, a flat ΛCDM universe with adiabatic primordial density perturbations, described by 6 cosmological parameters (Ω_Λ, ω_m, ω_b, A, n, τ). However, the data are no longer consistent with the 5-parameter "vanilla lite" model, i.e., one where the perturbations are scale-invariant, so that the parameter n would not be needed, since we now have $n < 1$ to "3 σ".

Actually the $n < 1$ claim assumes $r = 0$, since there is some degeneracy in the determination of n and r. The data is marginally (only 2σ away) consistent with $n = 1$ combined with large tensor perturbations, $r \sim 0.1$. See Fig. 30.

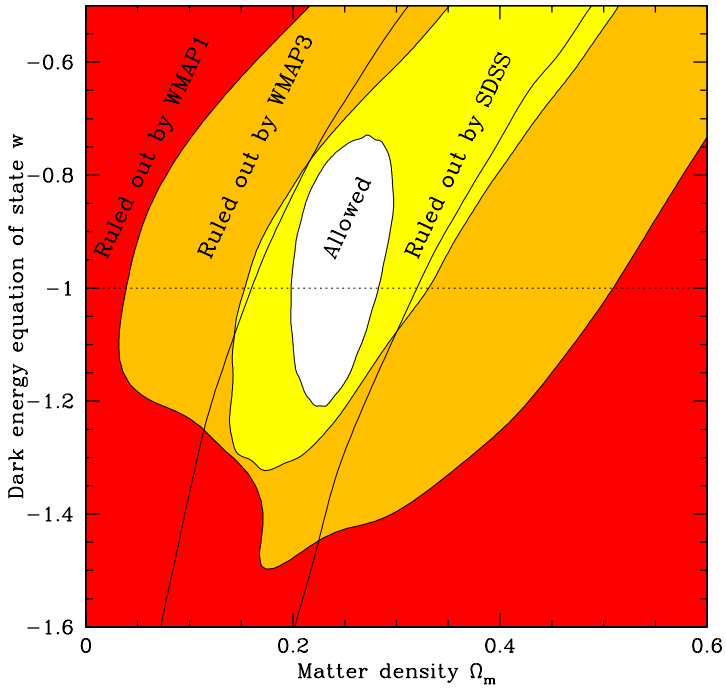

Figure 29: The SDSS data breaks the geometric degeneracy between $\Omega_\Lambda = 1 - \Omega_m$ and w in the WMAP3 data ($\Omega_0 = 1$ is assumed here). Figure from Tegmark et al. [10]

Future data with increasing accuracy, e.g., from the Planck satellite to be launched in 2009, holds the promise to significantly constrain inflation models by determining n, $dn/d\ln k$, and r more accurately. Also the Gaussianity and adiabaticity of primordial perturbations will be checked more accurately. Perhaps cosmology will also be able to determine the neutrino masses, instead of just giving upper limits. A most exciting discovery would be if it turned out that dark energy is not just a cosmological constant, i.e., that $w \neq -1$.

References

[1] C.L. Bennett et al., *First Year WMAP Observations: Preliminary Maps and Basic Results*, astro-ph/0302207, Astrophys. J. Suppl., 148, 1 (2003).

[2] D.N. Spergel et al., *WMAP Three Year Results: Implications for Cosmology*, astro-ph/0603449, Astrophys. J. Suppl., 170, 377 (2007)

[3] G. Hinshaw et al., *Five-Year WMAP Observations: Data processing, Sky Maps, & Basic results*, arXiv:0803.0732

[4] E. Komatsu et al., *Five-Year WMAP Observations: Cosmological Interpretation*, arXiv:0803:0547

[5] A.R. Liddle and D.H. Lyth: Cosmological Inflation and Large-Scale Structure (Cambridge University Press 2000).

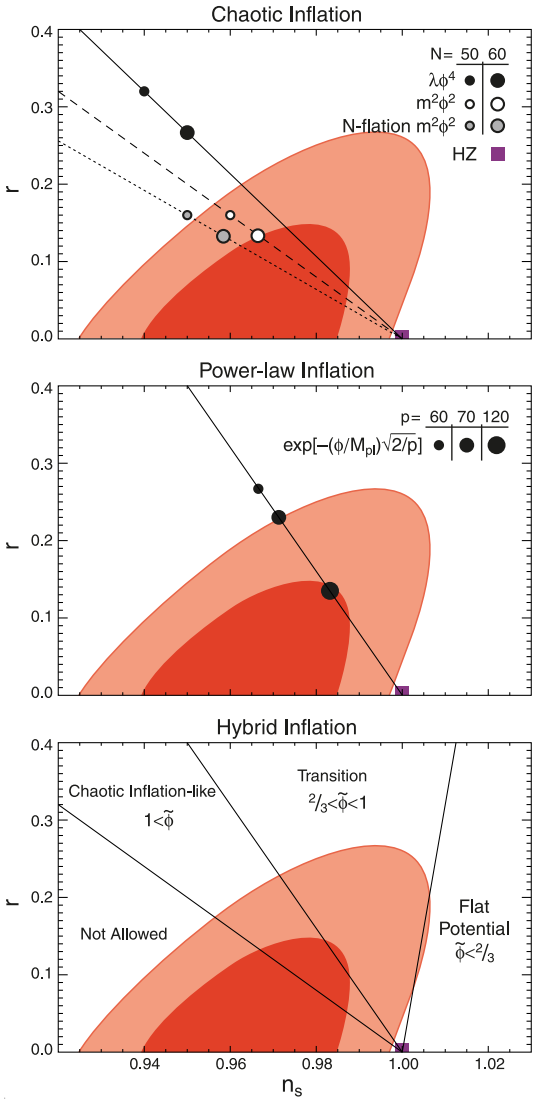

Figure 30: The WMAP5 constraints on the scalar perturbation spectral index n, and the tensor/scalar ratio r, when tensor perturbations are allowed. Some models which have large tensor perturbations are marked on the plots. We see that the $V(\varphi) \propto \varphi^4$ model is ruled out. The $V(\varphi) \propto \varphi^n$ models are often called "chaotic inflation" models, since they are usually connected to the idea of the universe emerging from the "spacetime foam" with "chaotic" initial conditions. Figure from [4].

[6] S. Dodelson: Modern Cosmology (Academic Press 2003).

[7] C. Reichardt et al., *High Resolution CMB Power Spectrum from the Complet ACBAR Data Set*, arXiv:0801.1491

[8] M. Roos, *Best median values for cosmological parameters*, astro-ph/0509089

[9] J. Väliviita, *PhD thesis*, University of Helsinki 2005.

[10] M. Tegmark et al., *Cosmological Constraints from the SDSS Luminous Red Galaxies*, astro-ph/0608632, Phys. Rev. D74, 123507 (2006).

[11] W.J. Percival et al., *Measuring the Baryon Acoustic Oscillation scale using the Sloan Digital Sky Survey and 2dF Galaxy Redshift Survey*